Available online at www.sciencedirect.com

SCIENCE DIRECT®

Coastal Engineering 51 (2004) 1021–1049

Coastal Engineering
An International Journal for Coastal, Harbour and Offshore Engineers

www.elsevier.com/locate/coastaleng

Analysis of some key parametrizations in a beach profile morphodynamical model

Karine Spielmann, Dominique Astruc*, Olivier Thual

Institut de Mécanique des Fluides de Toulouse, UMR 5502 CNRS/INPT-UPS, Allée du professeur Camille Soula, 31400 Toulouse, France

Received 27 January 2003; received in revised form 1 July 2004; accepted 16 July 2004
Available online 15 September 2004

Abstract

A numerical process-based model to forecast beach profile morphodynamics has been developed. In the present paper, an analysis of various modelling approaches and key parametrizations involved in the estimation of the wave-driven current and the suspended sediment concentration is carried out.

Several resolution techniques for the 1DV horizontal (i.e., in the x-direction perpendicular to coastline) momentum equation governing the Mean Horizontal Velocity (MHV) are analysed. In the first kind of techniques, the mean horizontal velocity is computed from the momentum equation, whereas the Mean Water Level (MWL) is computed using a parametrization of the depth-averaged momentum equation. Two boundary or integral conditions are thus needed. In the second kind, both mean horizontal velocity and mean water level gradient in the x-direction are the unknowns of the momentum equation, thus, three boundary or integral conditions are needed. Various additional conditions are discussed. We show that using a technique of the first kind is equivalent to imposing the difference between the surface and the bottom shear stresses in the 1D vertical equation. Both techniques lead to results that are in good agreement with the Delta Flume experimental data, provided the Stokes drift flow discharge is imposed as an additional condition. The influence of the breaking roller model and of the turbulent viscosity parametrization are also analysed.

Suspended sediment transport by the mean current and wave-induced bedload transport are taken into account in the sediment flux. Three turbulent diffusivity parametrizations are compared for suspended sediment concentration estimations. A linear profile for the turbulent diffusivity taking into account the wave bottom shear stress and the surface wave breaking turbulence production is shown to give the best results. Using experimental data, we put forward the poor estimation of the bottom sediment concentration given by the three implemented parametrizations. We thus propose a new parametrization relying on a Shields parameter based on the breaking roller induced surface shear stress. Using this new parametrization, the bottom profile used in the tests keeps its two bars which disappear otherwise. However, the morphodynamical model still overestimates the bars offshore motion, a bias already observed in other models.

Keywords: Beach profile; Morphodynamical model; Sediment transport; Bottom concentration

* Corresponding author. Tel.: +33 561 28 58 61; fax: +33 561 28 59 90.
E-mail address: astruc@imft.fr (D. Astruc).

0378-3839/$ - see front matter © 2004 Elsevier B.V. All rights reserved.
doi:10.1016/j.coastaleng.2004.07.020

1. Introduction

Modelling beach profile changes under the action of waves and currents has been a major concern in coastal research over the past decades and several numerical morphodynamical models have been developed for this purpose.

A review of these models has been performed by Roelvink and Brøker (1993) with a special emphasis on the so-called "deterministic" or "process-based" cross-shore models which explicitly take into account the various physical processes involved in beach profile dynamics. In such models, the wave field and the wave-driven current are computed across the profile in the shoaling and surf zones (Fig. 1). The sediment fluxes due to waves and currents are then estimated to compute the bottom evolution. These models proved to give valuable results for beach profile modelling during erosive storm events.

A deterministic beach profile morphodynamical model is usually based on four coupled submodels (Fig. 2): (i) a wave model (a breaking roller parametrization may be included), (ii) a current and mean water level (MWL) model, (iii) a sediment transport model and (iv) a bed evolution model. In most of the existing cross-shore models, submodels (i) to (iii) are stationary. It means that all the physical quantities are in equilibrium with the forcing terms and the boundary values. More recently, "phase-resolving" models taking into account the wave period variability have been developed (Rakha, 1998). However, this kind of models offers almost the same features for sediment transport and morphological evolution with an additional computer effort.

Although most of the "process-based" models share the same structure and almost the same governing equations, they proved to give scattered results when used to forecast the morphodynamics of barred beaches (Roelvink and Brøker, 1993; Srinivas and Dean, 1996). These differences may be due to the algorithms used to solve the governing equations, the parametrizations of the physical processes which cannot be explicitly resolved by the model or the numerical implementation.

In the present current and mean water level model, several techniques can be used to estimate the main outputs which are the Mean Horizontal Velocity (MHV) $\bar{u}(x, z)$ and the MWL $\bar{\eta}(x)$. These techniques can be classified into two main types: (i) the 1DV momentum equation is solved for $\bar{u}(x, z)$ only using two additional (boundary or integral) conditions. The gradient of the MWL $\bar{\eta}(x)$ in x-direction is estimated externally, either from data when available or more likely from an approximate depth integrated horizontal momentum equation. This kind of technique has been advocated by Svendsen et al. (1987). (ii) $\bar{u}(x, z)$ and $\bar{\eta}(x)$ are both computed from the momentum equation (Eq. (10)) so that three additional conditions are needed. This kind of technique has been used by De Vriend and Stive (1987). Of course, within each type of resolution techniques, an additional degree of freedom is given by the choice of the two or three conditions required to close the system. One possible condition is to impose the mean flow discharge in order to balance the Stokes drift. Boundary conditions should also be used. At the bottom, a Dirichlet type condition (either no-slip condition (Svendsen et al., 1987) or imposed mean velocity (Hansen and

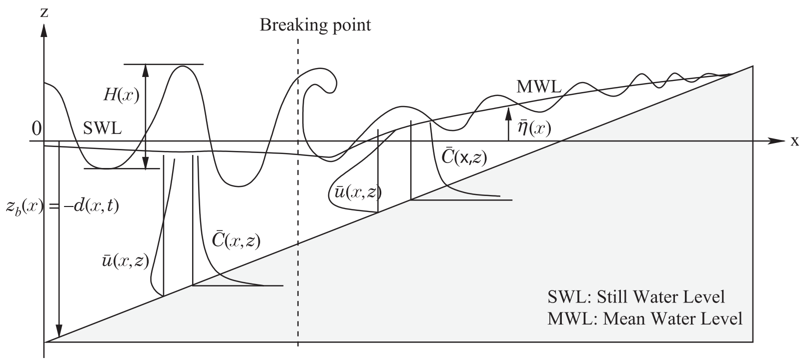

Fig. 1. Sketch of the domain.

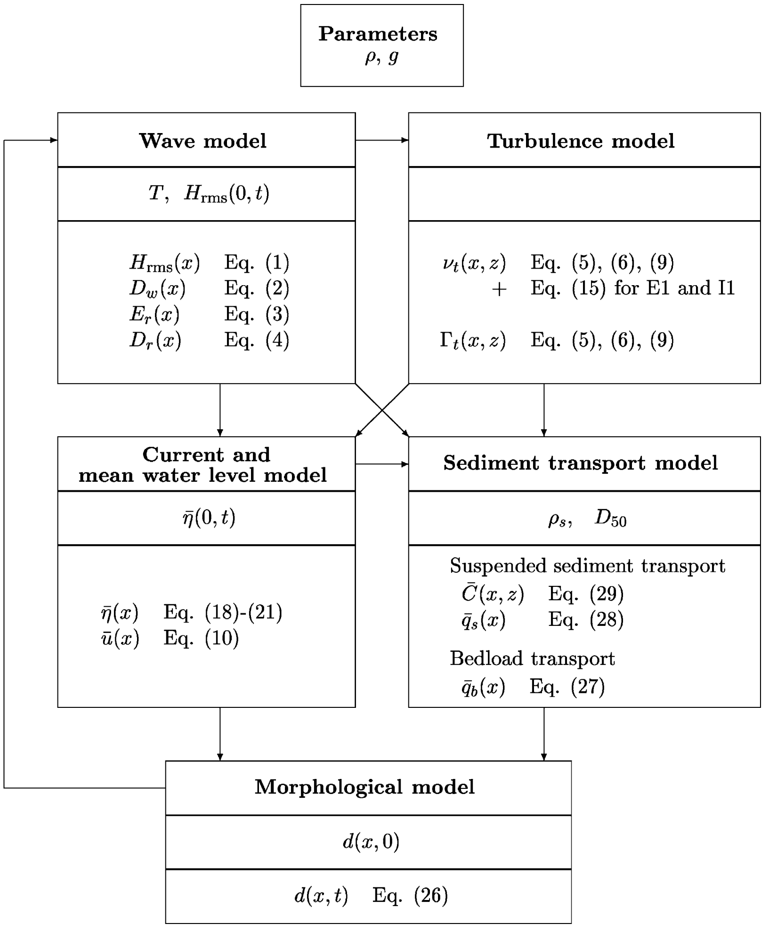

Fig. 2. Structure of the morphodynamical model.

Svendsen, 1984)) or a Neumann type condition (zero bed shear stress (Srinivas and Dean, 1996)) can be imposed. At the fluid surface, the only meaningful boundary condition is an imposed shear stress (Stive and Wind, 1986). Additional conditions have to be selected among these different conditions. The first goal of the present study is to analyse the sensitivity of the current and mean water level model output to the type of resolution technique and to the set of additional conditions used.

An important issue raised by previous studies is the modelling of the so-called transition zone effects by the introduction of a breaking roller. The transition zone, located between the shoaling zone and the inner surf zone, where the broken waves are similar to turbulent bores, was first reported by Svendsen et al. (1978). The transition zone features a rapid wave decay and a mean water level minimum shifted shoreward of the breaking point location. In a classical wave transformation model, wave breaking dynamics cannot be computed explicitly and has to be parametrized (Svendsen, 1984a). A breaking roller model may be used to take into account the transition zone effects in terms of mean flow (Stive and De Vriend, 1994). The roller is mainly characterized by its energy density $E_r(x)$ and dissipation rate $D_r(x)$. These two quantities can be used in the current and mean water level model and in the sediment transport model to estimate (i) the flow discharge involved in the integral mass flux condition (Svendsen, 1984a), (ii) the water surface shear stress (Deigaard and Fredsøe, 1989) when this kind of additional boundary condition is used, (iii) the roller induced momentum flux if a depth-integrated momentum equation is used, (iv) the turbulent viscosity (Battjes, 1983; Haines and Sallenger, 1994) and (v) the bottom sediment concentration (Smith and Mocke, 1993; present study). The second goal of this paper is to analyse the roller contribution in the estimation of mean velocity and mean water level. The parametrization of the breaking roller itself (cf. Svendsen, 1984a; Roelvink and Stive, 1989; Nairn et al., 1990) will not be discussed here.

The horizontal momentum equation includes a parametrization of the turbulent motion by means of a diffusion term. Although turbulence models such as k–L (Deigaard et al., 1991; Rakha, 1998) or $\bar{k}$–$\bar{\epsilon}$ (Mocke et al., 1994) models may be used, their superiority upon simpler 0-equation closures in the surf zone where the flow complexity is tremendous is not fully established. Thus, 0-equation models are still commonly used (Haines and Sallenger, 1994; Srinivas and Dean, 1996). Two different sources of turbulent motion are present in the surf zone: wave and current bottom shear stress and wave breaking which generates turbulence under the water surface (Battjes, 1983; Haines and Sallenger, 1994). These two contributions should be taken into account in the turbulent viscosity model (De Vriend and Stive, 1987) and different parametrizations for the turbulent viscosity have been proposed. The third goal of this paper is to analyse the impact of the turbulent viscosity parametrization on the mean flow properties.

The sediment transport model computes the distribution of the Mean Suspended Sediment Concentration (MSC) $\bar{C}(x, z)$ which results from a balance between turbulent diffusion and gravity driven sedimentation. Although simpler in its structure than the momentum equation, the governing equation for sediment distribution should be supplemented with two boundary conditions. At the water surface, a no flux condition is usually imposed (the vertical sediment flux may be non-zero if aeolian sand transport is to be accounted for). In addition, a boundary value for the suspended sediment concentration at some reference level close to the bottom, $\bar{C}_a(x)$, has to be imposed as a second boundary condition. This condition plays a central role in the suspended sediment distribution. The parametrization of $\bar{C}_a(x)$ has been the subject of a vast body of literature and is still an unresolved question in the surf zone. These parametrizations usually rely on the wave bottom shear stress (Nielsen, 1986; Van Rijn, 1989) whereas the effect of the breaking roller has also be introduced (Smith and Mocke, 1993). The fourth goal of this paper is to compare the results of these three $\bar{C}_a(x)$ parametrizations to experimental data. A new parametrization based on a Shields parameter $\theta_{\mathrm{s,r}}$ computed from the breaking roller surface shear stress is proposed and tested in this study.

Naturally, the parametrization of the turbulent diffusivity of the suspended sediment concentration is also a key point in the sediment model. The parametrizations for the turbulent diffusivity used in the present study are similar to those used for the turbulent viscosity.

In order to investigate the questions that we just raised, we have developed a deterministic beach profile model featuring a four submodels structure. This model includes some flexibility with respect to the resolution techniques and the physical parametrizations that we mentioned above so that several key parametrizations (turbulent viscosity and diffusivity, bottom concentration) and resolution techniques (resolution techniques for the momentum equation, breaking roller) are analysed. The methodology for this analysis is twofold. First, the influence of a particular modelling option on the model results is inferred from a direct comparison of the related model output with the experimental data. Second, in addition to this direct and local analysis, some insights into the global influence of a given modelling option on the final output of the morphodynamical model are gained by the analysis of cross-shore sediment fluxes distribution and bottom profiles.

The paper is organized as follows. The Delta Flume'93 (Arcilla et al., 1994) experimental data set used for comparison purposes is presented in the next section. The wave model is introduced and validated in Section 3. In Section 4, the three different parametrizations for the turbulent diffusion coefficients which have been implemented are introduced. In Section 5, the various resolution techniques used in the current and mean water level model are detailed and analysed. The sensitivity analysis of the current and mean water level model results to the resolution techniques, the roller terms and the turbulence closure are presented in Section 6. The sediment transport model is introduced in Section 7 as well as the new bottom sediment concentration parametrization. In Section 8, the influence of the turbulent diffusivity model and the bottom sediment concentration parametrizations on the suspended sediment distributions are analysed. Then, in Section 9, the impact of the modelling options on cross-shore sediment fluxes and beach cross-shore profiles is evaluated. Finally, conclusions are drawn in the last section.

2. Experimental data set for model validation

The Delta Flume'93 experiments (Arcilla et al., 1994; Roelvink and Reniers, 1995) have been performed in a large-scale wave flume to provide high-quality data sets for deterministic beach profile models calibration and validation. The experiments consist in a sandy bottom exposed to various random wave conditions.

The flume was equipped with several instruments fixed on the wall: two surface-following wave gauges near the wave generator in order to estimate the incident wave characteristics, ten pressure sensors positioned below the wave trough level, and five velocity meters attached at different x-locations. Moreover, a mobile carriage which can be moved during the experiment was equipped with an automatic sounding system to measure the bottom profile, five electromagnetic current meters and ten sediment concentration suction tubes located at fixed vertical positions to provide the vertical structure of the MHV and the MSC.

Every hour of a given test, wave height, mean water level and bottom position are measured along the profile whereas the MHV and the MSC vertical profiles are measured over the water depth at a single cross-shore position.

In the present study, the highly erosive regime of Test 1b is used for comparison purposes. During this test, the bottom profiles exhibit two sandbars which grow and move seaward with time (see Fig. 3). The offshore (x_0=20 m) root mean square wave height $H_{rms,0}$ and mean water level η_0 are kept almost constant during the test (Table 1). The physical parameters are given in Table 2. Fig. 3 shows the location of the movable carriage used to measure

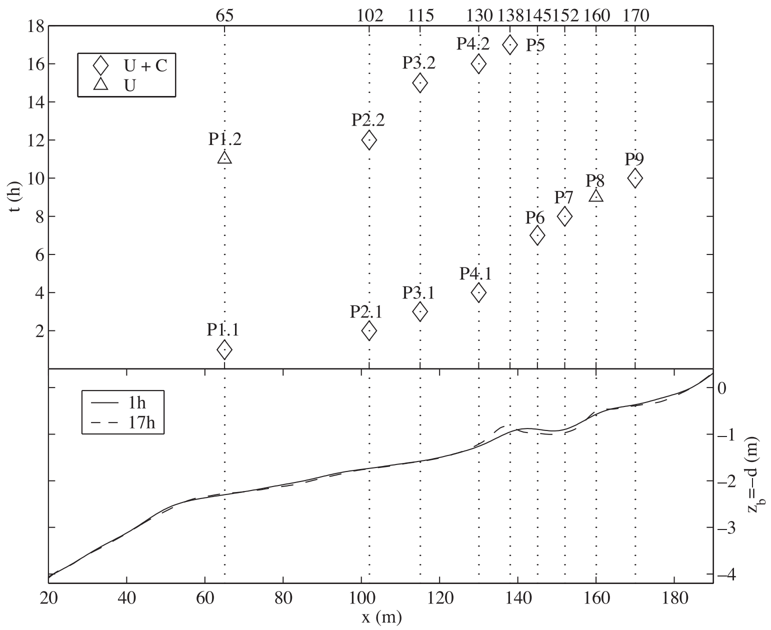

Fig. 3. Top: Space and time locations of the P_i vertical profiles measurements performed during Test 1b of the Delta Flume experiments (Arcilla et al., 1994), (△) only $\bar{u}(x_i, z)$ is measured, (◇) both $\bar{u}(x_i, z)$ and $\bar{C}(x_i, z)$ are measured. Bottom: Measured sea-bed profiles $-d(x)$ at (—) t=1 h and (– –) t=17 h.

Table 1
Overview of measurements performed during Test 1b of the Delta Flume experiments

t (h)	$H_{rms,0}$ (m)	$\bar{\eta}_0$ (m)	Performed measurements	Measurements location (m)
1	0.928	−0.0538	$\bar{u}(z)$ and $\bar{C}(z)$	65
2	0.927	−0.0614	$\bar{u}(z)$ and $\bar{C}(z)$	102
3	0.926	−0.0762	$\bar{u}(z)$ and $\bar{C}(z)$	115
4	0.931	−0.093	$\bar{u}(z)$ and $\bar{C}(z)$	130
5	–	−0.037	–	138
6	–	−0.0414	–	–
7	0.981	−0.0471	$\bar{u}(z)$ and $\bar{C}(z)$	145
8	0.985	−0.0513	$\bar{u}(z)$ and $\bar{C}(z)$	152
9	0.987	−0.0496	$\bar{u}(z)$	160
10	0.985	−0.0521	$\bar{u}(z)$ and $\bar{C}(z)$	170
11	0.984	−0.0476	$\bar{u}(z)$	65
12	0.981	−0.049	$\bar{u}(z)$ and $\bar{C}(z)$	102
13	0.988	−0.04	–	–
14	0.983	−0.0478	–	–
15	0.981	−0.0487	$\bar{u}(z)$ and $\bar{C}(z)$	115
16	0.988	−0.0463	$\bar{u}(z)$ and $\bar{C}(z)$	130
17	0.986	−0.0492	$\bar{u}(z)$ and $\bar{C}(z)$	138

$H_{rms,0}$: Offshore wave height measured at x_0=20 m; $\bar{\eta}_0$: offshore MWL at x_0=20 m.

vertical profiles of the MHV and the MSC during the Test 1b experiment.

3. Wave model

The wave model computes the wave field across the beach profile, using either a linear or a non-linear wave theory. In addition, the breaking roller characteristics are computed using the parametrization of Stive and De Vriend (1994). The wave characteristics (height and period) are required at the seaward boundary.

3.1. Wave transformation model

The wave height $H_{rms}(x)$ is computed across the beach profile from either the linear wave theory or the first-order cnoidal wave theory using the wave energy flux balance:

$$\frac{\partial\left[C_g(x)E_w(x)\right]}{\partial x} = -D_w(x)$$
$$\text{with } E_w(x) = f\left(H_{rms}^2(x)\right) \qquad (1)$$

where $C_g(x)$ is the wave group velocity, $E_w(x)$ the wave energy per surface unit which may be related to $H_{rms}(x)$ according to the selected wave theory and $C_g(x)E_w(x)$ the wave energy flux.

The Battjes and Janssen (1978) model which takes into account the randomness of the wave height is used to estimate the wave energy dissipation rate $D_w(x)$:

$$D_w(x) = \frac{1}{4}\rho g \alpha H_{max}^2(x)Q_b(x)/T_p \qquad (2)$$

where ρ is the water density, g the gravitational acceleration, α an order-one empirical coefficient, $H_{max}(x)$ the maximum wave height defined by the breaking criteria (Battjes and Stive, 1985), $Q_b(x)$ the fraction of broken wave and T_p the peak wave period.

The cnoidal wave integral properties have been inferred from Hardy and Kraus (1987).

3.2. Breaking roller model

The roller energy per surface unit $E_r(x)$ is computed from the balance between the wave energy dissipation rate, $D_w(x)$, and the roller energy dissipation rate, $D_r(x)$ (Stive and De Vriend, 1994):

$$\frac{\partial\left[2C_\varphi(x)E_r(x)\right]}{\partial x} = D_w(x) - D_r(x) \text{ with } E_r(x_0) = 0 \qquad (3)$$

where $C_\varphi(x)$ is the wave phase velocity as the roller is supposed to travel on the top of each wave crest and x_0=20 m the offshore position for Delta Flume experiments (Fig. 3).

The parametrization for $D_r(x)$ used in the present model has been proposed by Nairn et al. (1990):

$$D_r(x) = 2\beta g\frac{E_r(x)}{C_\varphi(x)} \qquad (4)$$

where β is a coefficient related to the wave steepness (usually β=0.1).

Table 2
Model parameters and seaward boundary conditions

Inputs		Model parameters	
$H_{rms,0}$	see Table 1	β	0.1
$\bar{\eta}_0$	see Table 1	M	0.025
$d(x, t_i)$	measured	κ	0.41
ρ	1000 kg/m^3	c_f	0.01
ρ_s	2650 kg/m^3	ϵ_b	0.21
D_{50}	2×10^{-4} m	c_d	0.01
D_{90}	2.47×10^{-4} m	Φ	32°
Δx	0.5 m	n_z	200

3.3. Wave model validation

Fig. 4a shows the cross-shore profile of $H_{rms}(x)$ measured at the last hour of Test 1b and computed using the linear theory. The wave height is in good agreement with the measurements despite a slight overestimation in the trough between the two longshore bars ($x \simeq 150$ m). We have also observed that the cross-shore profile of $H_{rms}(x)$ keeps the same shape all over the test: the wave amplitude slightly increases from seaward until $x \simeq 50$ m which is the location of the bottom slope change where the waves start to break. Then, the wave height slowly decreases until the shoreline with two regions of stronger decrease over the bars ($x \simeq 140$ m and $x \simeq 160$ m).

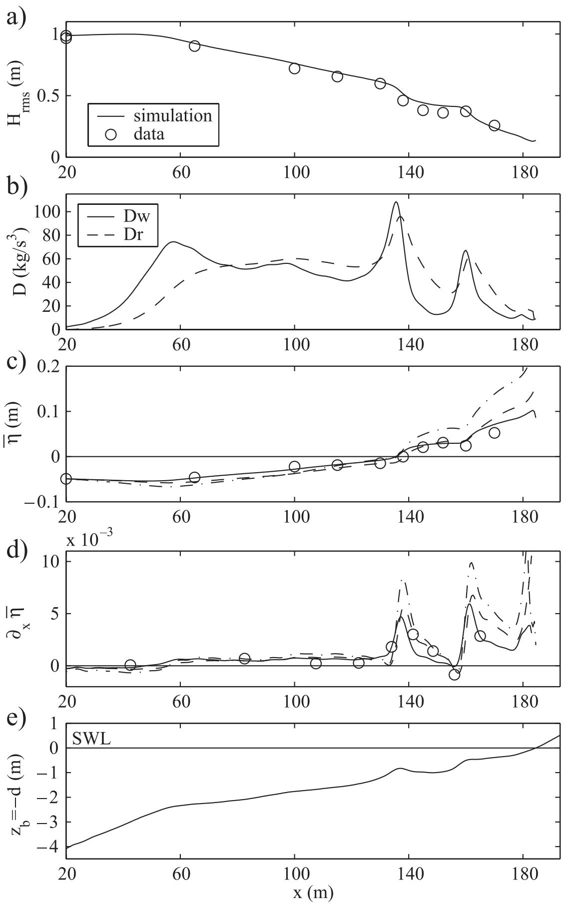

Fig. 4. Cross-shore profiles at t=17 h. (a) Wave height $H_{rms}(x)$: (—) model, (○) experimental data. (b) (—) Wave dissipation rate $D_w(x)$, (– –) roller dissipation rate $D_r(x)$. (c) Mean Water Level (MWL) $\bar{\eta}(x)$: (—) E2 without roller contribution (Eq. (18)), (– –) E2 with roller contribution (Eq. 21)), (– · –) I2, (○) experimental data. (d) Gradient of the MWL in x-direction $\partial_x\bar{\eta}(x)$: (—) E2 without roller contribution (Eq. (18)), (– –) E2 with roller contribution (Eq. (21)), (– · –) I2, (○) experimental data. (e) Measured bed profile. The same profiles are obtained if E1 is replaced by E2 or I1 by I2.

This behaviour is in agreement with the cross-shore profile of the wave dissipation rate $D_w(x)$ (Fig. 4b) which exhibits three maxima, one at the slope change ($x \simeq 50$ m) and two at the bars location. The roller dissipation rate $D_r(x)$ exhibits a cross-shore distribution which has many common features with the $D_w(x)$ profile. However, two significant differences can be quoted: first, there is no local maximum for $D_r(x)$ at $x \simeq 50$ m as $D_r(x)$ shows increasing values from seaward until the outer bar. Second, the two maxima of roller dissipation observed over the bars are located 1.5 m closer to the shoreline than the maxima of $D_w(x)$. This shift is remanent of the lag in turbulence injection by wave breaking which occurs across the transition zone (Roelvink and Stive, 1989).

4. Turbulence modelling

The Reynold stress term in the momentum equation (Eq. (10)) is modelled by a first-order closure using the turbulent viscosity $\bar{\nu}_t(x, z)$ concept. In the mean suspended concentration equation (Eq. (29)), the turbulent diffusivity $\bar{\Gamma}_t(x, z)$ is also used to model the fluctuating velocity and concentration correlation term (see Section 7.3).

The turbulent diffusion coefficient $\mathcal{D}_t(x,z)$ (either $\bar{\nu}_t$ or $\bar{\Gamma}_t$) is modelled using a 0-equation approach. Three different vertical profiles for $\mathcal{D}_t(x,z)$ have been implemented to test the relative effect of the two main sources of turbulence, i.e., the wave induced bottom shear stress and the wave breaking.

4.1. First model: $\mathcal{D}_{t,1}(x)$

In order to take into account the wave breaking induced turbulence, Battjes (1983) related the turbulent viscosity at a given cross-shore location to the local wave energy dissipation rate, $D_w(x)$ (see also Haines and Sallenger, 1994). However, Roelvink and Stive (1989) conjectured that the turbulent kinetic energy resulting from the wave breaking is not immediately dissipated. This lag between production and dissipation should be modelled by a storage term in the wave energy flux conservation equation (Eq. (1)). In the present model, this storage takes place in the roller whose energy balance is governed by Eq. (3). The turbulent viscosity should therefore be computed from the roller dissipation rate $D_r(x)$ instead of the wave energy dissipation (Deigaard et al., 1991; Mocke et al., 1994; Rakha, 1998). The simplest model is a uniform turbulent diffusion over the water depth:

$$\mathcal{D}_{t,1}(x) = Md(x)\left(\frac{D_r(x)}{\rho}\right)^{\frac{1}{3}} \tag{5}$$

where $d(x)$ is the water depth (Fig. 1), ρ the fluid density and M a constant. De Vriend and Stive (1987) showed that a good agreement with Svendsen (1987) data is obtained for M=0.025.

4.2. Second model: $\mathcal{D}_{t,2}(x)$

De Vriend and Stive (1987) supplemented the $\mathcal{D}_{t,1}$ model with the bottom friction contribution to the turbulent viscosity. The bottom friction term they considered is uniform over the depth and proportional to the friction velocity $u_*(x)$:

$$\mathcal{D}_{t,2}(x) = \kappa u_*(x)d(x) + Md(x)\left(\frac{D_r(x)}{\rho}\right)^{\frac{1}{3}} \tag{6}$$

where κ=0.41 is the Karman constant and $u_*(x)$ the friction velocity.

In the present study, the mean current bottom shear stress is neglected and the friction velocity $u_*(x)$ is equal to the wave friction velocity $u_w(x) = \sqrt{\frac{\bar{\tau}_{b,max}(x)}{\rho}}$. The maximum bottom shear stress $\bar{\tau}_{b,max}(x)$ is computed (using the linear wave theory) from:

$$\bar{\tau}_{b,max}(x) = \frac{1}{2}\rho f_w(x)\tilde{u}_b^2(x) \tag{7}$$

with $\tilde{u}_b(x)$ the amplitude of the near-bottom wave velocity and $f_w(x)$ the wave-friction coefficient, assumed to be constant over a wave cycle and modelled by (Swart, 1976):

$$f_w(x) = \exp\left[-6 + 5.2\left(\frac{A(x)}{k_s}\right)^{-0.19}\right] \tag{8.a}$$

for $A(x)/k_s$>1.57

$$f_{w,max} = 0.3 \quad \text{for } A(x)/k_s \leq 1.57 \tag{8.b}$$

where k_s=2D_{50} is the Nikuradse roughness height (Kamphuis, 1975) with D_{50} the median diameter of bed material, and $A(x)$=$\tilde{u}_b(x)/\omega$ the wave orbital excursion (from linear theory) with ω the radian frequency.

4.3. Third model: $\mathcal{D}_{t,3}(x,z)$

Grant and Madsen (1979) proposed instead to use a bottom friction contribution which varies linearly with the depth. Combining both turbulence sources, we propose:

$$\mathcal{D}_{t,3}(x,z) = \kappa u_*(x)(z + d(x)) + Md(x)\left(\frac{D_r(x)}{\rho}\right)^{\frac{1}{3}} = \mathcal{D}_{t,2}(x) + \kappa u^*(x)z \tag{9}$$

5. Current and mean water level model

The current and mean water level model computes the MHV distribution $\bar{u}(x, z)$ and the MWL $\bar{\eta}(x)$ at each cross-shore location. The wave and breaking roller characteristics are required from the wave model, as well as the mean water level at the seaward boundary (see Fig. 1).

5.1. Wave-averaged horizontal momentum equation

To derive an equation for the MHV, the instantaneous horizontal velocity is decomposed into three components, the wave averaged velocity or MHV $\bar{u}(x, z)$ which is the unknown here, the periodic component corresponding to the wave motion $\tilde{u}(x, z, t)$ and the turbulent fluctuation $u'(x, z, t)$. This decomposition is introduced in the horizontal momentum equation which is next averaged over a wave period assuming that $\bar{u}$ and u' are uncorrelated (i.e., very different characteristic time scales for the wave and the turbulent fluctuations) so that $\overline{\tilde{u}u'}$=0. Then, the Reynolds turbulence modelling and the standard expression for the mean pressure, $\bar{P}(x,z) = \rho g(\bar{\eta}(x) - z) - \rho\overline{\tilde{w}^2}(x,z)$, with $\tilde{w}$ the vertical wave orbital velocity component (Stive and Wind, 1986), are introduced. Finally, only the steady motion and the vertical processes are retained in the model since the hydrodynamics of the surf zone is dominated by wave breaking and related turbulent kinetic energy injection from the water surface. Both horizontal advection and diffusion processes are thus neglected. The MHV field $\bar{u}(x, z)$ is therefore governed by (for details, see Nielsen, 1992, Chap. 1, pp. 60–61):

$$\frac{\partial}{\partial z}\left(\bar{\nu}_{t}(x,z)\frac{\partial \bar{u}(x,z)}{\partial z}\right) = g\frac{\partial \bar{\eta}(x)}{\partial x} + \frac{\partial\left(\overline{\tilde{u}^{2}}(x,z) - \overline{\tilde{w}^{2}}(x,z)\right)}{\partial x} \tag{10}$$

where $\bar{\nu}_t(x, z)$ is one of the parametrizations for $\mathcal{D}_t(x,z)$ (Section 4).

In the present study, the additional term $\partial_z\overline{\tilde{u}\tilde{w}}(x,z)$ which should appear in the right-hand side of Eq. (10) is neglected as we do not focus here on the explicit resolution of the bottom boundary layer (BBL) (Stive and Wind, 1986). Its contribution may be, however, important in this area (De Vriend and Kitou, 1990; Deigaard et al., 1991). Moreover, recent studies show that the magnitude of this term in the surf zone is not yet well known (Cox and Kobayashi, 1996) so that its modelling is still an open question (Rivero and Arcilla, 1995, 1997; You, 1996, 1997). However, we have performed some numerical tests which show that the effect of this term (evaluated from Longuet-Higgins', 1953 parametrization) is of secondary importance compared to the effect of the techniques used to solve Eq. (10).

5.2. Resolution techniques

Various resolution techniques have been proposed for Eq. (10) which may be sorted into two main types.

5.2.1. Type E

Eq. (10) governs only the MHV, whereas the forcing term $\partial_x\bar{\eta}(x)$ is computed "externally" (E) from the depth averaged momentum conservation equation (Eq. (18) or (21)). Thus, two additional conditions are required to solve Eq. (10) in terms of $\bar{u}(x, z)$. These additional conditions may be of integral type (flow discharge condition) or boundary conditions (at the surface or at the bottom). Three possible choices among the set of additional conditions lead to E0 (Hansen and Svendsen, 1984; Srinivas and Dean, 1996), E1 (Svendsen et al., 1987; Haines and Sallenger, 1994) and E2 (Srinivas and Dean, 1996) techniques (see Table 3):

5.2.2. Type I

The MHV $\bar{u}(x, z)$ and the MWL $\partial_x\bar{\eta}(x)$ are both "internal" (I) unknowns in Eq. (10), so three additional conditions are then required. Two different choices for the additional conditions lead to both I1 and I2 techniques (see Table 3). This kind of approach has been proposed by De Vriend and Stive (1987) and is used in several deterministic models (e.g., Roelvink and Stive, 1989; Roelvink and Brøker, 1993).

Whatever resolution technique is used, the breaking roller contribution may also be included.

The three different types of boundary conditions are introduced in Section 5.4. For E type techniques, the complete problem requires the estimation of the mean water level which is described in Section 5.5. Let us now introduce the integral condition for the MHV $\bar{u}(x, z)$.

5.3. Flow discharge condition

There is a general consensus about the fact that, for an accurate undertow estimation, the depth-integrated mass balance equation should be used as one condition (e.g., Stive and Wind, 1986). This condition states that the undertow should balance the shoreward mass flux induced by the wave motion and possibly by the breaking roller, as the net cross-shore water mass flux is equal to zero.

In the present model, two different mass balance conditions are implemented, in order to put forward

Table 3
Choice of the boundary conditions and/or equations to solve Eq. (10)

	Mass flux (Eq. (11))	No slip (Eq. (14))	No stress ((Eq. (17))	Surface stress (Eq. (13))	MWL (Eqs. (18)–(21))
E0	×			×	×
E1	×	×			×
E2	×		×		×
I1	×	×		×	
I2	×		×	×	

the breaking roller influence on the MHV vertical profiles:

$$\int_{-d(x)}^{0} \bar{u}\,(x,z)\mathrm{d}z = -\frac{E_{\mathrm{w}}(x)}{\rho C_{\varphi}(x)} \tag{11.a}$$

$$\int_{-d(x)}^{0} \bar{u}\,(x,z)\mathrm{d}z = -\frac{E_{\mathrm{w}}(x)+2E_{\mathrm{r}}(x)}{\rho C_{\varphi}(x)} \tag{11.b}$$

Eq. (11.a) only takes into account the wave mass flux (Stokes drift), whereas Eq. (11.b) includes the roller contribution as well (Svendsen, 1984b).

5.4. Additional boundary conditions

Among the possible boundary conditions, three have been considered in the present study.

5.4.1. Surface shear stress condition

Seaward of the surf zone, the surface shear stress is only due to wind action and is usually overlooked for nearshore applications leading to a null shear stress condition at the surface. In the surf zone, however, the wave breaking induces a downward horizontal momentum transfer from the fluid above the wave trough, which contributes to the driving force for the mean flow (Stive and Wind, 1986). This horizontal momentum flux should be taken into account by a shear stress at the water surface. Stive and Wind (1986) proposed a parametrization of the surface shear stress $\bar{\tau}_{\mathrm{s}}(x)$, including the roller contribution (Svendsen, 1984a,b):

$$\bar{\tau}_{\mathrm{s}}(x) = -\left(\frac{1}{2}+\frac{2E_{\mathrm{r}}(x)}{E_{\mathrm{w}}(x)}\right)\frac{\partial E_{\mathrm{w}}(x)}{\partial x}. \tag{12}$$

In the present study, the parametrization proposed by Deigaard and Fredsøe (1989) is used instead:

$$\bar{\tau}_{\mathrm{s}}(x) = \rho\bar{v}_{\mathrm{t}}(x,0)\frac{\partial \bar{u}\,(x,0)}{\partial z} = \frac{D_{\mathrm{r}}(x)}{C_{\varphi}(x)}. \tag{13}$$

5.4.2. Bottom no-slip condition (with bottom boundary layer resolution)

A no-slip condition at the sea-bed can also be used as an additional boundary condition:

$$\bar{u}\,(x,-d) = 0. \tag{14}$$

According to Svendsen et al. (1987), this condition should be used together with a turbulent viscosity model (called $\bar{v}_{\mathrm{tb}}$) which features very small values inside the BBL. In the present model, the uniform over the BBL parametrization for $\bar{v}_{\mathrm{tb}}$ proposed by Stive and De Vriend (1987) is used:

$$\bar{v}_{\mathrm{tb}}(x) = c_{\mathrm{f}}^{2}\tilde{u}_{\mathrm{b}}^{2}(x)/\omega \text{ for } z< -d(x)+\delta_{\mathrm{w}}(x) \tag{15}$$

where $\delta_{\mathrm{w}}(x)$ is the wave BBL thickness and c_{f} a friction coefficient which depends on the bottom roughness. Stive and De Vriend (1987) used Eq. (15) in the BBL and Eq. (5) outside (with D_{w} instead of D_{r}). The sensitivity analysis they performed shows that the results are weakly dependent on the c_{f} value (here c_{f}=0.01).

The wave BBL thickness $\delta_{\mathrm{w}}(x)$ is estimated using (Jonsson and Carlsen, 1976):

$$\frac{30\delta_{\mathrm{w}}(x)}{k_{\mathrm{s}}}\log\left(\frac{30\delta_{\mathrm{w}}(x)}{k_{\mathrm{s}}}\right) = 1.2\frac{A(x)}{k_{\mathrm{s}}}$$

which is equivalent to (Jonsson and Carlsen, 1976):

$$\frac{\delta_{\mathrm{w}}(x)}{k_{\mathrm{s}}} = 0.072\left(\frac{A(x)}{k_{\mathrm{s}}}\right)^{-0.25}. \tag{16}$$

5.4.3. Bottom shear stress condition

Using the bottom no-slip condition, Svendsen et al. (1987) found that the bottom shear stress is negligible in the bed vicinity, so that $\bar{\tau}_{\mathrm{b}}(x)$=0 at the bottom is a reasonably accurate approximation. Similar conclusions were drawn using laboratory experiments (Ting and Kirby, 1994).

A zero bottom shear stress condition at the top of the BBL should be used as a bottom boundary condition for Eq. (10). As the BBL thickness is very small compared to the depth, this condition can also be imposed at the sea-bed for convenience (Srinivas and Dean, 1996):

$$\bar{\tau}_{\mathrm{b}}(x) = \rho\bar{v}_{\mathrm{t}}(x,-d)\frac{\partial \bar{u}\,(x,-d)}{\partial z} = 0. \tag{17}$$

5.5. Mean water level estimation

If an E type resolution technique for Eq. (10) is used, the external specification of the pressure term

$\partial_x\bar{\eta}(x)$ is required. Although $\partial_x\bar{\eta}(x)$ may sometimes be given by experimental data (Stive and Wind, 1986), this MWL gradient is usually estimated using an approximate depth-integrated horizontal momentum equation, assuming no mass flux and no bottom shear stress. Then, the MWL gradient balances the gradient of the radiation stress $S_{\mathrm{xx,w}}(x)$ (Stive and Wind, 1986):

$$\rho g d(x)\frac{\partial\bar{\eta}(x)}{\partial x}+\frac{\partial S_{\mathrm{xx,w}}(x)}{\partial x}=0. \tag{18}$$

The radiation stress $S_{\mathrm{xx,w}}(x)$ is the excess of momentum flux due to wave motion, pressure and turbulent fluctuations:

$$S_{\mathrm{xx,w}}(x)=\rho\overline{\int_{-d}^{\eta}\left[\tilde{u}^2(x,z,t)-\tilde{w}^2(x,z,t)\right]\mathrm{d}z}+\frac{1}{2}\rho g\overline{[\eta(x,t)-\bar{\eta}(x)]^2} \tag{19}$$

$$=\left[\frac{2C_{\mathrm{g}}(x)}{C_{\varphi}(x)}-\frac{1}{2}\right]_{E_{\mathrm{w}}(x)}$$

(for the linear wave model). (20)

As we already noticed, the breaking roller momentum flux may also be accounted for in the balance of Eq. (18) (Svendsen, 1984a):

$$\rho g d(x)\frac{\partial\bar{\eta}(x)}{\partial x}+\frac{\partial\left(S_{\mathrm{xx,w}}(x)+S_{\mathrm{xx,r}}(x)\right)}{\partial x}=0 \tag{21}$$

where the roller radiation stress $S_{\mathrm{xx,r}}(x)$ is parametrized by (Svendsen, 1984a):

$$S_{\mathrm{xx,r}}(x)=2E_{\mathrm{r}}(x). \tag{22}$$

5.6. Some comments on the resolution techniques for Eq. (10)

Before proceeding to the numerical tests, we analyse the five mathematically relevant resolution techniques considered in this study (Table 3). In particular, we want to put forward the similarities between E and I types of resolution techniques.

Integrating Eq. (10) from the bed level to the Still Water Level (SWL, z=0) and using Leibniz's rule as well as the definition of $S_{\mathrm{xx,w}}(x)$ (Eq. (19)), one obtains:

$$\begin{aligned}\rho g d(x)\frac{\partial\bar{\eta}(x)}{\partial x}&-[\bar{\tau}_{\mathrm{s}}(x)-\bar{\tau}_{\mathrm{b}}(x)]\\&=-\frac{\partial S_{\mathrm{xx,w}}(x)}{\partial x}+\frac{1}{2}\frac{\partial E_{\mathrm{w}}(x)}{\partial x}+\rho(\overline{\tilde{u}^2}(x,-d)\\&\quad-\overline{\tilde{w}^2}(x,-d))\frac{\partial d(x)}{\partial x}.\end{aligned} \tag{23}$$

If an E type resolution technique is used, the MWL gradient is estimated from Eq. (18) or (21). Then, combining Eq. (18) or (21) with Eq. (23), we get:

$$\begin{aligned}\bar{\tau}_{\mathrm{s}}(x)-\bar{\tau}_{\mathrm{b}}(x)=&-\frac{1}{2}\frac{\partial E_{\mathrm{w}}(x)}{\partial x}-\rho(\overline{\tilde{u}^2}(x,-d)\\&-\overline{\tilde{w}^2}(x,-d))\frac{\partial d(x)}{\partial x}\end{aligned} \tag{24}$$

or

$$\begin{aligned}\bar{\tau}_{\mathrm{s}}(x)-\bar{\tau}_{\mathrm{b}}(x)=&-\frac{\partial S_{\mathrm{xx,r}}(x)}{\partial x}-\frac{1}{2}\frac{\partial E_{\mathrm{w}}(x)}{\partial x}\\&-\rho(\overline{\tilde{u}^2}(x,-d)-\overline{\tilde{w}^2}(x,-d))\\&\times\frac{\partial d(x)}{\partial x}\end{aligned} \tag{25}$$

This result enables us to make some important comments on the resolution techniques:

(1) E0: Eq. (10) is solved using the flow rate condition (Eqs. (11a) and (11b)) and the surface shear stress condition (Eq. (13)), whereas Eq. (18) or (21) is used to compute the MWL. Thus, we should notice that the bottom shear stress governed by Eq. (24) or (25) is not vanishing at all. E0 technique is not physically correct since the bottom shear stress may experience large non zero values unlike both experimental and numerical observations in the surf zone. Some numerical tests (not reported in details in the present paper), shown that the vertical profile of the MHV is poorly estimated, $\bar{\tau}_{\mathrm{b}}(x)$ ranging between -10 and 10 N m^{-2}. These numerical results confirm that E0 technique does not give a proper estimation of $\bar{u}(x,z)$.

(2) E1 or E2: Bottom boundary conditions (Eq. (14) for E1 or Eq. (17) for E2) are used to solve Eq. (10) together with the flow rate condition. Therefore, Eq. (24) or (25) governs the value

of the resulting surface shear stress as $\bar{\tau}_b$, computed from the MHV, is negligible for E1 (because of the small value of the turbulent viscosity $\bar{v}_{tb}$) and vanishes for E2. Although not explicitly imposed, the surface shear stress is therefore controlled by the parametrization of the MWL gradient. The so-called "external" condition, Eq. (18) or (21), can be viewed as an additional condition for the mean surface shear stress, $\bar{\tau}_s(x)$. Thus, Eq. (25) is an alternative parametrization for $\bar{\tau}_s(x)$ which should be compared to the parametrization proposed by Stive and Wind (1986) (Eq. (12)) or by Deigaard and Fredsøe (1989) (Eq. (13)).

(3) I1 or I2: The flow discharge condition is combined with both surface shear stress condition (Eq. (13)) and Eq. (14) (I1) or Eq. (17) (I2) for the bottom boundary condition. In this case, the MWL gradient is governed by Eq. (23). As expected, the resolution of Eq. (10) for MHV and MWL leads to a different estimation for the MWL gradient than the depth averaged equation (Eq. (18) or (21)).

6. Current and MWL model sensitivity analysis

A set of tests is performed to analyse the influence of some model features on the $\bar{\eta}(x)$ and $\bar{u}(x, z)$ estimation: (i) resolution techniques (E1, E2, I1 or I2), (ii) breaking roller parametrization, (iii) turbulent viscosity parametrization. The analysis is conducted first for the MWL estimation ((i) and (ii) only) and then for the horizontal velocity field.

6.1. Mean water level estimation

Four different estimations for the MWL $\bar{\eta}(x)$ and its gradient in x-direction $\partial_x\bar{\eta}(x)$ are performed at the 17th hour of Test 1b: (a) $\partial_x\bar{\eta}(x)$ is computed using Eq. (18) as a balance between the gradients of the MWL and the wave radiation stress only (like in E type techniques), (b) Eq. (21) is used so that the roller momentum flux is included in the $\partial_x\bar{\eta}(x)$ estimation, (c) I1 technique is used to estimate $\partial_x\bar{\eta}(x)$ from Eq. (10), (d) $\partial_x\bar{\eta}(x)$ is estimated from Eq. (10) using I2 technique. As the results obtained from I1 and I2 techniques are almost the same, only I2 results are presented here.

The experimental values of the gradient of the MWL in the x-direction (Fig. 4d) are computed from the available MWL measurements although we should bear in mind that their poor resolution near the shoreline leads to some inaccuracies, like the absence of a maximum for $\partial_x\bar{\eta}(x)$ over the shoreward bar.

6.1.1. Influence of the resolution technique

The results obtained using the various techniques (Fig. 4c and d) are in agreement with the experimental data seaward of the outer bar. In this region, E type techniques proved to be slightly more accurate. From the outer bar to the shoreline, $\bar{\eta}(x)$ and $\partial_x\bar{\eta}(x)$ are overestimated when I type techniques are used, whereas better results are obtained with E type techniques (Eq. (18) or (21)). Despite the sparsity of the data which do not allow to conclude on the quantitative accuracy of E type techniques, they provide a more reliable estimate than I type techniques.

6.1.2. Breaking roller influence

The results from E1 technique, with either Eq. (18) or (21), are compared to experimental data (Fig. 4c). The computed MWL exhibits almost the same behaviour in good agreement with the experimental data. A deeper analysis shows that the roller term slightly reduces the MWL from the offshore boundary to the crest of the inner bar ($x \simeq 160$ m) to provide a better fit with the experimental data in this area. One can observe that the change in slope of $\bar{\eta}(x)$ at the outer bar is located shoreward when the roller is accounted for. The MWL is however overestimated shoreward of the inner bar (from $x \simeq 170$ m to the shoreline) when the roller term is included. A better agreement is observed without it, although $\bar{\eta}(x)$ remains slightly overestimated.

The roller influence is more significant on the MWL gradient in x-direction (Fig. 4d). Without the roller term, the two maxima of $\partial_x\bar{\eta}(x)$ are located over the bars crest, whereas when the roller is taken into account, the value for the $\partial_x\bar{\eta}(x)$ maxima is increased and their locations are shifted shoreward, so that a better agreement with experimental data is gained. The model properly represents the storage effect due to the roller, which can be viewed as the time needed by the roller to develop.

From these observations, we conclude that the breaking roller has to be taken into account in the depth-averaged momentum equation (Eq. (21)) to accurately estimate $\bar{\eta}(x)$ and $\partial_x\bar{\eta}(x)$. We also recall that I1 and I2 techniques significantly overestimate $\bar{\eta}(x)$ and $\partial_x\bar{\eta}(x)$, especially in the bars area.

6.2. Mean horizontal velocity estimation

6.2.1. Resolution techniques

In order to analyse the impact of the resolution technique on the MHV estimation, four tests have been performed using E1, E2, I1 and I2 techniques. In all these computations, the roller terms are taken into account in the MWL estimation for E type techniques and in the flow discharge condition (Eq. (11.b)). The $\bar{\nu}_{t,2}$ turbulent viscosity model (Eq. (6)) is used.

In Fig. 5, the MHV profiles $\bar{u}(z)$ at the measurement cross-shore locations (Fig. 3) are plotted. Whatever the technique used, the vertical profiles of the MHV feature a seaward directed current as expected in the surf zone. Some comments on the shape of these vertical profiles should be done.

The mean velocity gradient at the bottom is zero for E2 and I2 techniques as a consequence of the null bottom shear stress condition (Eq. (17)). When the no-slip condition (Eq. (14)) is used instead (E1 and I1), the profiles feature a non zero bottom shear stress at the top of the bottom boundary layer which is, however, very small, of the order of -5×10^{-4} N m^{-2}. These observations confirm that both additional conditions (Eqs. (14) and (17)) are almost equivalent (Svendsen et al., 1987). We will, however, more likely use the zero bottom shear stress condition (E2 and I2) as the no-slip condition requires two additional parametrizations (for the BBL thickness and the turbulent viscosity in the vicinity of the bed $\bar{\nu}_{tb}$) which introduce an additional complexity in the model.

Seaward of the outer bar (from $P_{1.1}$ to $P_{4.2}$) and shoreward of the inner bar (P_8 and P_9), the modulus of the MHV is overestimated for all the techniques. For I type resolution techniques, however, this overestimation is greater than for E type techniques. At P_6 and P_7

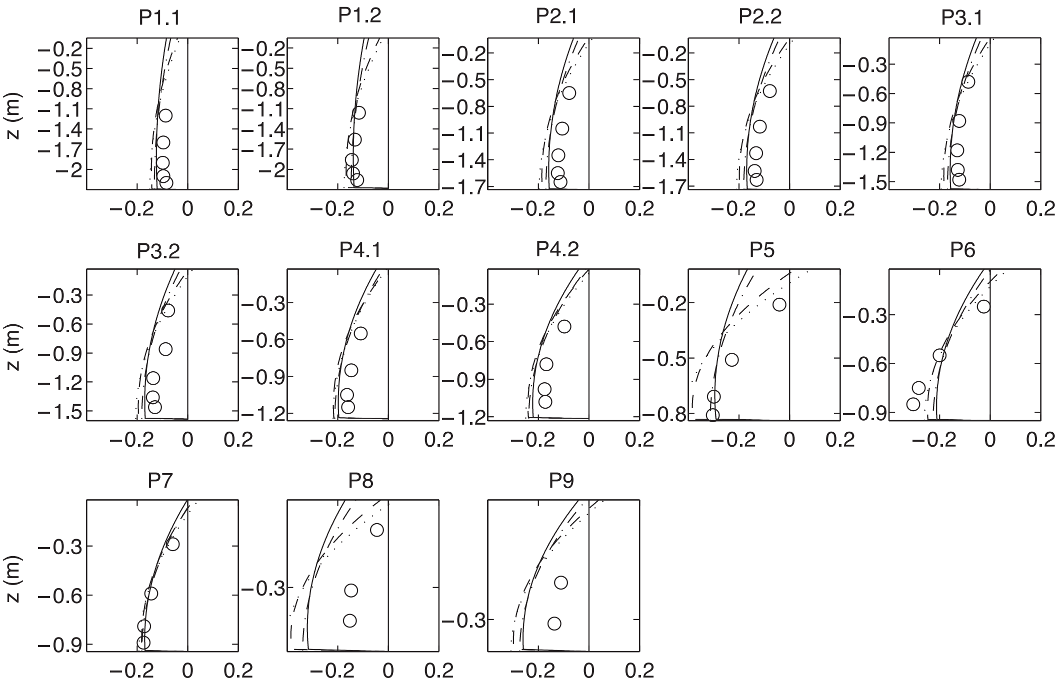

Fig. 5. Vertical profiles of the Mean Horizontal Velocity (MHV) $\bar{u}(x, z)$ when the roller term is included in the integral condition (Eq. (11.b)) (m/s). (—) E1, (– · –) E2, (– –) I1, (· · ·) I2, (○) experimental data.

(in the trough), a small difference can be observed, with nevertheless a better agreement for I type techniques at P_6. At P_5, the shape of the vertical structure of $\bar{u}(x, z)$ seems to be better evaluated using I techniques whereas the intensity of $\bar{u}(x, z)$ (especially near the bottom) is better estimated with E techniques.

It can also be observed that the mean velocity gradient at the surface is better estimated using I type techniques. The additional surface shear stress condition (Eq. (13)) seems therefore to be an accurate parametrization of the momentum transfer due to the breaking roller. However, the velocity gradient obtained with E type techniques features a reasonable behaviour, with better values near the bottom.

In conclusion, I1 and I2 techniques lead to an overestimation of $\bar{u}(x, z)$ when the roller is accounted for, but the shape of the vertical profiles of $\bar{u}(x, z)$ is properly estimated for all cross-shore positions. Using E1 and E2 techniques, the velocity magnitude seems to be better estimated, especially in the vicinity of the bed, although still overestimated at almost all the locations. The vertical profile is, however, more uniform than the profile obtained with I techniques leading to a less accurate estimation, especially when the wave breaking is important. We also show that E1 and E2 (or I1 and I2) give almost similar results, E2 (or I2) being preferred for its simplicity.

6.2.2. Breaking roller influence

We now analyse the breaking roller influence on the vertical profiles of the MHV for both types of technique, E and I.

6.2.2.1. E type conditions. In the E2 technique, the roller contribution is taken into account in two equations, Eq. (21) for the MWL and Eq. (11.b) for the flow discharge. In order to analyse the impact of this contribution on the vertical profiles of $\bar{u}$(x, z), three tests have been performed using the $\bar{\nu}_{t,2}$ turbulent viscosity:

E2R11—the roller term is included in both mass balance condition (Eq. (11.b)) and depth averaged momentum equation (Eq. (21)),

E2R10—the roller term is included in the depth averaged momentum Eq. (21) only,

E2R00—the roller is not taken into account.

The comparison of the vertical profiles of $\bar{u}(x, z)$ (Fig. 6) shows that the overestimation of the MHV obtained with E2R11 is mainly due to the roller contribution in the mass conservation condition (Eq. (11.b)). Using E2R10, $\bar{u}(x, z)$ magnitudes are smaller, whereas the vertical structure remains the same as the one obtained with E2R11. E2R10 results are in good agreement with experiments from P_2 to P_4 and at P_7, P_8 and P_9. At the other locations, the undertow is, however, underestimated when E2R10 is used.

We now compare the E2R00 and E2R10 model results in details, for each experimental profiles in order to understand the impact of the roller contribution in the $\partial_x\bar{\eta}(x)$ estimation. At P_1, the best results are obtained when the roller terms are not introduced at all (E2R00). The vertical structure as well as the magnitude are better estimated using E2R00, in particular for the gradient close to the surface whereas the bottom values remain too strong. At P_2, P_3, P_4 and P_8, only a slight difference is observed between E2R00 and E2R10 results. In fact, the values of $\partial_x\bar{\eta}(x)$ at these locations are very similar (see Fig. 4d). At P_9, the E2R00 model results are very close to the data with an almost homogeneous profile across the depth, whereas the profile obtained with E2R10 is similar to the one obtained at P_8. This difference is due to the forcing term $\partial_x\bar{\eta}(x)$ in Eq. (10) which is smaller when the roller contribution is not accounted for (Fig. 4d) and thus better estimated. It is, however, in the bars area (at P_5, P_6 and P_7) that the difference between E2R10 and E2R00 results is very important. Indeed, the E2R00 results exhibit an almost uniform vertical profile with smaller values compared to the data. This behaviour shows that it is necessary to take into account the additional momentum flux due to the roller in the MWL estimation (i.e., E2R10) in order to obtain accurate vertical profiles for the undertow.

In order to clarify the behaviour of $\bar{u}(x, z)$, the cross-shore distribution of the surface shear stress $\bar{\tau}_s(x)$ is analysed for each technique. Reference values for $\bar{\tau}_s(x)$ have been computed from the $\bar{u}(x, z)$ experimental values and the $\bar{\nu}_t$ values given by the $\bar{\nu}_{t,2}$ parametrization. These values lead to an approximation of the experimental values but cannot give a good quantitative reference.

Cross-shore profiles of $\bar{\tau}_s(x)$ (Fig. 7) obtained with E2R00 and E2R11 (or E2R10 since the flow discharge condition (Eqs. (11a) and (11b)) does not influence

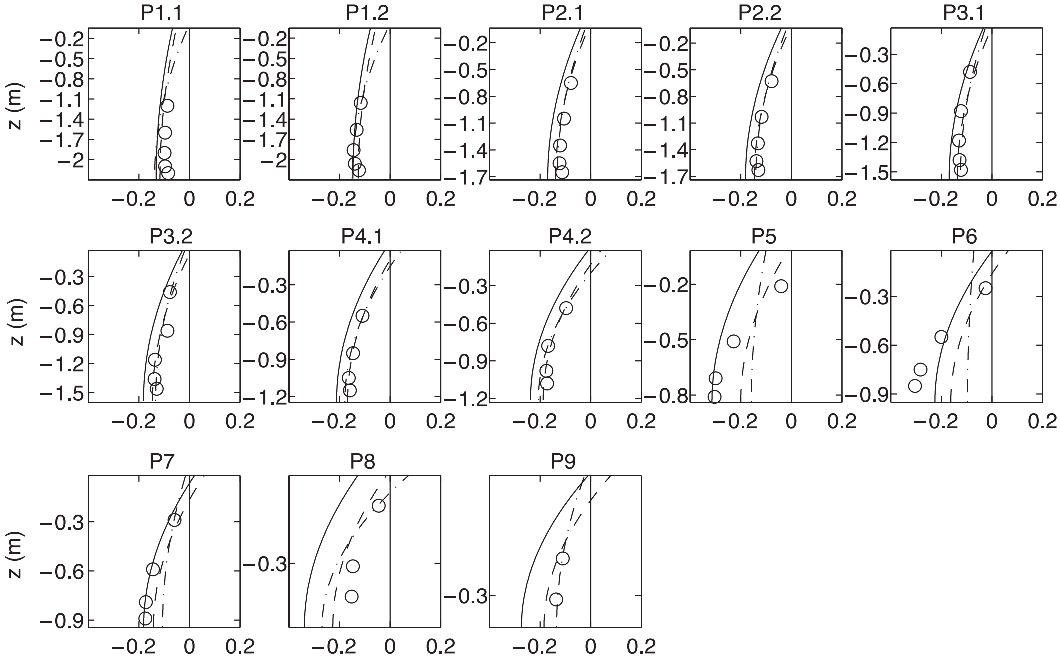

Fig. 6. Vertical profiles of the Mean Horizontal Velocity (MHV) $\bar{u}(x, z)$ (m/s). (—) E2R11(Eqs. (11.b) and (21)), (– –) E2R10 (Eqs. (11.a) and (21)), (– · –) E2R00 (Eqs. (11.b) and (18)), (○) experimental data.

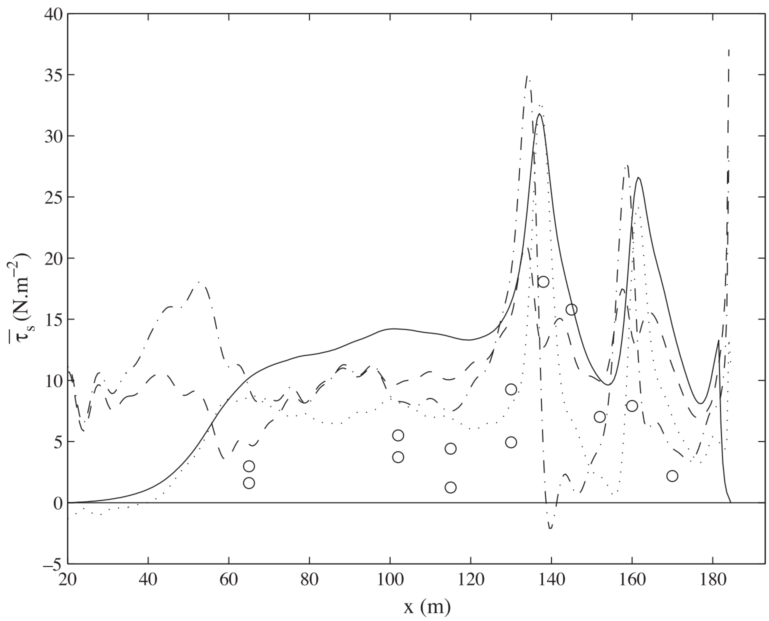

Fig. 7. Cross-shore profiles of the surface shear stress $\bar{\tau}_s(x)$ (N m^{-2}). (—) Eq. (13) (I2), (– –) Eq. (25) (E2R11), (– · –) Eq. (25) (E2R00), (· · ·) Eq. (12), (○) estimated reference values.

$\bar{\tau}_s(x)$) exhibit strong fluctuations seaward of the outer bar coming from the bed slope term in Eq. (25) and the wave energy gradient. The same behaviour is observed for the Stive and Wind (1986) parametrization (Eq. (12)). We should also notice that, in E2R00 and the Stive and Wind (1986) parametrization results, $\bar{\tau}_s(x)$ is negative at some locations, which is not physically acceptable. Moreover, we already discussed the poor estimation of the vertical profiles of $\bar{u}(x, z)$ using E2R00 at x=138 m (P_5) and x=145 m (P_6) which can be related to the small values of $\bar{\tau}_s(x)$ (≈ 4 N m^{-2} and ≈ 1.4 N m^{-2}, respectively). A strong difference between $\bar{\tau}_s(x)$ at x=65 m computed using E2R00 and E2R11 is observed which explains the difference observed in the behaviour of the vertical profiles of $\bar{u}(x, z)$. The E2R00 results are very close to the Deigaard and Fredsøe (1989) parametrization results and lead to the best fit for $\bar{u}(x, z)$. The cross-shore variability of $\bar{\tau}_s(x)$ seems to be properly estimated using the Deigaard and Fredsøe (1989) parametrization even if no quantitative agreement is obtained.

For all the resolution techniques except for E2 with the roller contribution, $\bar{\tau}_s(x)$ exhibits two maxima over the bars, which are very close in amplitude to those obtained with both classical parametrizations (Eqs. (12) and (13)). Using E2 type technique, they are located seaward, with the same shift already observed between $D_w(x)$ and $D_r(x)$. One should also notice that $\bar{\tau}_s(x)$ exhibits two maxima over each bar for E2R11 which has no clear physical meaning. However, the introduction of the roller term leads to a positive surface shear stress all over the profile, which allows to obtain better values for $\bar{\tau}_s(x)$ at x=138 m (P_5) and x=145 m (P_6) and thus, better vertical profiles for the MHV.

6.2.2.2. I type conditions. The roller contribution is only taken into account in the flow discharge condition (Eq. (11.a) or (11.b)) so only two tests are performed here, I2R11 using Eq. (11.a) and I2R00 using Eq. (11.b). In addition, the roller is used to estimate the surface shear stress since the Deigaard and Fredsøe (1989) parametrization (Eq. (13)) is retained in this study.

With the roller term (I2R11), the $\bar{u}(x, z)$ magnitude is overestimated, whereas the results are closer to the experimental data without the roller contribution (I2R00) (Fig. 8) (except at P_6 where the undertow is

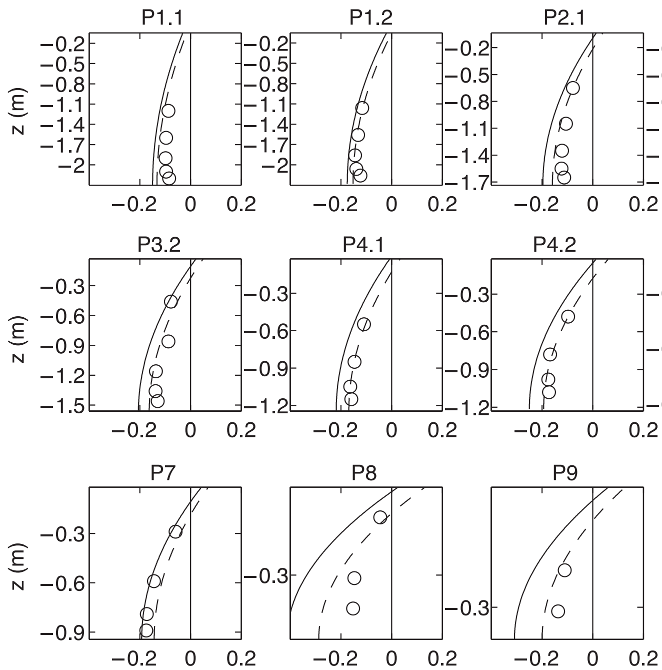

Fig. 8. Vertical profiles of the Mean Horizontal Velocity (MHV) $\bar{u}(x, z)$ (m/s). (—) I2R11 (Eq. (11.b)), (– –) I2R00 (Eq. (11.a)), (○) experimental data.

underestimated). Therefore, the mass flux induced by the roller can explain the overestimation of $\bar{u}(x, z)$ already noticed (Fig. 5). The I2R00 technique leads to a good estimation of the slope of $\bar{u}(x, z)$ near the surface whereas the bottom value is overestimated at almost all the locations, except at P_5, P_6 and P_7. The I2R00 results are in very good agreement with the experimental data at P_5 (x=138 m) where $\bar{\tau}_s(x)$ and $\partial_x\bar{\eta}(x)$ reach their maximum. However, the strong value of $\partial_x\bar{\eta}(x)$ gives a bad estimation of the MWL $\bar{\eta}(x)$ (Fig. 4c and d). At P_7 (x=152 m), the undertow is slightly underestimated as the roller mass flux is small in the trough area. This underestimation is even stronger at P_6 (x=145 m), the only profile where I2R11 gives the best results.

Thus, I2 type technique, based on the $\bar{\tau}_s(x)$ parametrization of Deigaard and Fredsøe (1989), gives good results for $\bar{u}(x, z)$ without the additional roller mass flux in the flow discharge condition (Eq. (11.a)) (I2R00).

The difference between the cross-shore profiles of $\bar{\tau}_s(x)$ (Fig. 7) estimated using Stive and Wind (1986) model (Eq. (12)) and using the one proposed by Deigaard and Fredsøe (1989) (Eq. (13)) allow us to conclude that the former parametrization will not give a proper estimation of the undertow, in particular, in the seaward region as $\bar{\tau}_s(x)$ is negative.

6.2.3. Influence of the turbulent viscosity model

In this section, the tests of the three turbulent viscosity models are performed using E2R11, i.e., using Eqs. (11.b) and (21).

The results obtained using $\bar{\nu}_{t,1}(x)$ (Fig. 9) feature an important overestimation of the MHV in the lower part of the water column, leading to unrealistic $\bar{u}(x, z)$ gradients at the fluid surface. This overestimation is even more important for I2 technique (not shown). The results are more accurate when the wave bottom friction turbulence production is included ($\bar{\nu}_{t,2}$ or $\bar{\nu}_{t,3}$). These turbulent viscosity models lead to slightly different $\bar{u}(x, z)$ vertical profiles, the best estimation being obtained with the $\bar{\nu}_{t,2}(x)$ uniform viscosity. In fact, the velocities near the bottom $\bar{u}(x, z)$ are smaller and better estimated with $\bar{\nu}_{t,2}(x)$ than with $\bar{\nu}_{t,3}$. A reliable estimation of near-bottom velocities is an

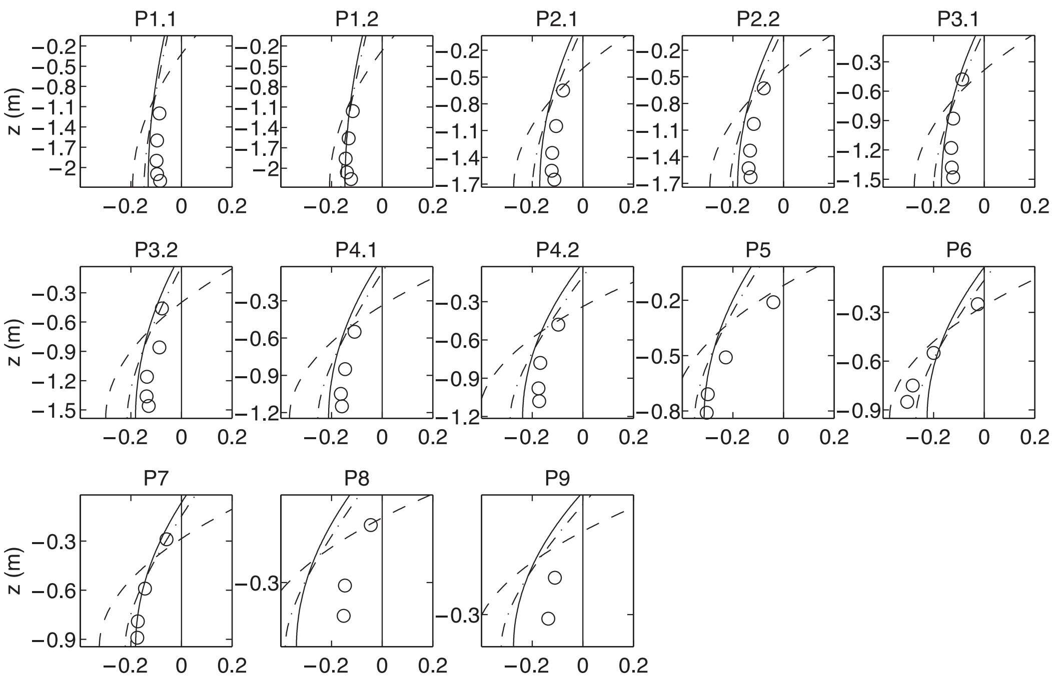

Fig. 9. Vertical profiles of the Mean Horizontal Velocity (MHV) $\bar{u}(x, z)$ (m/s), using E2. (– –) $\bar{\nu}_{t,1}(x)$: Eq. (5), (—) $\bar{\nu}_{t,2}(x)$: Eq. (6), (– · –) $\bar{\nu}_{t,3}(x, z)$: Eq. (9), (○) experimental data.

important criteria for suspended sediment transport computations.

These results highlight the need to take into account both turbulence generation mechanisms, bottom friction and wave breaking, in the turbulent viscosity parametrization. The $\bar{v}_{t,2}(x)$ uniform vertical profile, as suggested by Stive and Wind (1986), leads to the best results.

6.2.4. Summary

For both E and I types techniques, we show that a no slip condition compared to a null bottom shear stress condition at the bottom does not improve significantly the vertical profile of the MHV $\bar{u}(x, z)$ despite its additional numerical complexity.

In Fig. 10, one can see the main features of the different resolution techniques. First, the roller contribution term (E2R11 and I2R11) gives an overestimation of the MHV intensity, except in the trough area (P_5 and P_6) where I2 gives the best results. Second, I2R00 technique leads to an overestimation of the undertow in the vicinity of the bottom at P_2, P_3 and P_8 whereas accurate results are obtained with E2R10 technique, as the surface shear stress is smaller at these locations (Fig. 7). At P_1 and P_5, I2R00 gives the best results for $\bar{u}(x, z)$ (Fig. 6). In fact, the surface shear stress which reaches its maximum at P_5 is better estimated. The parametrization of Deigaard and Fredsøe (1989) based on the roller dynamics allows to properly fit the undertow profile when wave breaking is significant. Third, E2R10 and I2R00 give almost the same results at the other locations (P_4, P_6, P_7 and P_9), with almost similar values for $\bar{\tau}_s(x)$.

For E2 technique, we show that the roller term has to be taken into account in the estimation of the MWL (Eq. (21)). Finally, the difference between E2R10 and I2R00, which gives the best results, can be related to the surface shear stress estimation, which is better with I2 despite a bad estimation of the MWL.

Finally, we show that both turbulence productions from the bottom friction and the wave breaking have to be taken into account in the turbulent viscosity parametrization which has to be uniform along the depth.

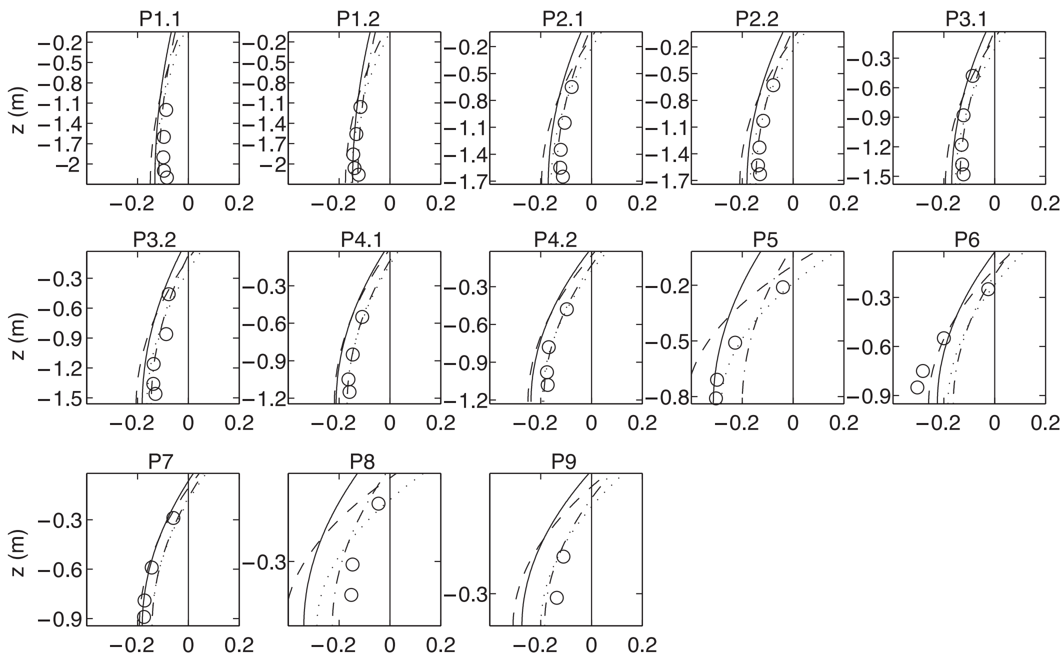

Fig. 10. Vertical profiles of the Mean Horizontal Velocity (MHV) $\bar{u}(x, z)$ (m/s). (—) E1R11, (– · –) E2R10, (– –) I1R11, (· · ·) I2R00, (○) experimental data.

7. Bottom evolution and sediment transport models

7.1. Morphological model

The bed evolution is computed according to the sediment conservation equation:

$$\frac{\partial d(x,t)}{\partial t} = (1+p)\frac{\partial \bar{q}_{\mathrm{t}}(x,t)}{\partial x} \tag{26}$$

where $\bar{q}_{\mathrm{t}}(x, t)$ is the total sediment flux and p the bed porosity. In this study, the effects of pores are neglected (p=0) like in other studies (Srinivas and Dean, 1996).

We follow Rakha et al. (1997) for the numerical scheme for Eq. (26) using a modified Lax scheme and a α_{d} coefficient taken to be 0.25 as they proposed.

Two contributions are taken into account to compute the total sediment flux $\bar{q}_{\mathrm{t}}(x)$: the bedload flux $\bar{q}_{\mathrm{b}}(x)$ induced by the wave bottom shear stress and the suspended flux $\bar{q}_{\mathrm{s}}(x)$ related to the wave-driven current, the undertow. The first one is estimated from an empirical formula whereas the second one is explicitly computed by the model.

7.2. Bedload transport

Many morphological models (Srinivas and Dean, 1996; Rakha et al., 1997; Roelvink and Brøker, 1993) rely on the Bailard and Inman (1981) transport formula to take into account the sediment transport due to the wave asymmetry. The Bailard and Inman (1981) wave period averaged bedload flux $\bar{q}_{\mathrm{b}}(x)$ (m^2/s) is:

$$\bar{q}_{\mathrm{b}}(x) = \frac{c_{\mathrm{d}}\epsilon_{\mathrm{b}}}{2g(s_{\mathrm{d}}-1)\tan\Phi}\left(\overline{|u_{\mathrm{t}}(x,-d,t)|^2 u_{\mathrm{t}}(x,-d,t)} - \frac{s(x)}{\tan\Phi}\,\overline{|u_{\mathrm{t}}(x,-d,t)|^3}\right) \tag{27}$$

with c_{d} the drag coefficient, ϵ_{b} the bedload efficiency factor, $s_{\mathrm{d}}=\rho_{\mathrm{s}}/\rho$ the specific gravity (with ρ_{s} the sediment density), Φ the dynamic friction angle (Φ=32°), $s(x)$ the local bed slope and $u_{\mathrm{t}}(x, -d, t)$ the time-dependent near-bottom fluid velocity. In the present model, the mean flow velocity is neglected and the wave bottom velocity is computed using the first-order cnoidal theory (Hardy and Kraus, 1987).

7.3. Suspended sediment transport

As we consider only the suspended sediment flux related to the undertow, the mean suspended sediment transport rate $\bar{q}_{\mathrm{s}}(x)$ is computed from the vertical profiles of $\bar{u}(x, z)$ and the MSC $\bar{C}(x, z)$:

$$\bar{q}_{\mathrm{s}}(x) = \frac{1}{\rho_{\mathrm{s}}}\int_{-d(x)}^{0} \bar{u}(x,z)\bar{C}(x,z)\mathrm{d}z. \tag{28}$$

The vertical distribution of $\bar{C}(x, z)$ is computed from an equilibrium between the turbulent diffusion and the gravity-driven sediment motion with a no mass flux condition at the sea surface:

$$\bar{\Gamma}_{\mathrm{t}}(x,z)\frac{\partial \bar{C}(x,z)}{\partial z} + w_{\mathrm{s}}\bar{C}(x,z) = 0 \tag{29}$$

where w_{s} is the sediment fall velocity. The turbulent diffusivity $\bar{\Gamma}_{\mathrm{t}}(x, z)$ is parametrized by Eq. (5), (6) or (9).

Eq. (29) requires a boundary condition at the bottom. In the present model, we impose the sediment concentration, $\bar{C}_a(x)$, at $z=a=-d+k_{\mathrm{s}}$ where k_{s} is the bottom roughness height. Four different parametrizations of $\bar{C}_a(x)$ are implemented including a new one.

7.3.1. Nielsen model—N86

The Nielsen (1986) empirical model relates $\bar{C}_a(x)$ to the Shields parameter $\theta_{\mathrm{s}}(x)$:

$$\bar{C}_a(x) = 0.005\rho_{\mathrm{s}}\theta_{\mathrm{s}}(x)^3 \text{with } \theta_{\mathrm{s}}(x) = \frac{\bar{\tau}_{\mathrm{b,max}}(x)}{(\rho_{\mathrm{s}}-\rho)gD_{50}} \tag{30}$$

where D_{50} is the median sediment diameter and $\bar{\tau}_{\mathrm{b,max}}(x)$ the maximum bottom shear stress induced by the wave motion (Eq. (7)).

7.3.2. Van Rijn model—VR89

According to the empirical parametrization proposed by Van Rijn (1989), $\bar{C}_a(x)$ is a function of $T_a(x)$, the non-dimensional excess of bottom shear stress:

$$\bar{C}_a(x) = 0.015\rho_{\mathrm{s}}\frac{D_{50}}{k_{\mathrm{s}}}\frac{T_a(x)^{1.5}}{D_{\star}^{0.3}} \text{if } T_a(x)0 \tag{31.a}$$

$$= 0 \text{ if } T_a(x)<0 \tag{31.b}$$

where $D_\star = D_{50}\left[\frac{(s_d-1)g}{v^2}\right]^{1/3}$ is the particle diameter and ν the kinematic viscosity (10^{-6} m^2/s). In this model, $T_a(x)=(\tau'_b(x)-\tau_{b,cr})/\tau_{b,cr}$ where $\tau'_b(x)$ is the bed shear stress related to the grains which represents the fraction of the bed-shear stress devoted to sediment transport, $\tau'_b(x)=\mu_a\bar{\tau}_b(x)$ (with μ_a=Max(0.06, 0.6/D$_\star$) and $\bar{\tau}_b(x)=\bar{\tau}_{b,max}(x)$). $\bar{\tau}_{b,cr}=\rho_s-\rho)\times gD_{50}\theta_{cr}$ is the critical bed shear stress where θ_{cr} is computed from D$_\star$ using the Shields curve.

7.3.3. Smith and Mocke model—SM93

Smith and Mocke (1993) proposed to take into account the wave breaking contribution to the bottom concentration, using the roller energy dissipation rate:

$$\bar{C}_a(x) = A\theta_s(x) + B\frac{D_r(x)}{\rho}. \tag{32}$$

The two coefficients A=2.16 kg/m^3 and B=21.35 kg.m/s^3 were calibrated using several near-bed concentrations measurements in the surf zone.

7.3.4. A new model—SAT01

The breaking roller plays an important role on the hydrodynamics of the surf zone, at least in the vicinity of the bars as we showed in the current and MWL model analysis. The breaking roller contribution should therefore be taken into account in the parametrization of $\bar{C}_a(x)$. Instead of using the roller dissipation rate like Smith and Mocke (1993), we propose to relate $\bar{C}_a(x)$ to the sea-surface shear stress induced by the roller $\bar{\tau}_{s,r}(x)$. We thus propose a parametrization which relies on the Shields parameter $\theta_{s,r}(x)$ built with $\bar{\tau}_{s,r}(x)$:

$$\bar{C}_a(x)=\alpha_c\rho_s\theta^3_{s,r}(x) \text{ with } \theta_{s,r}(x)=\frac{\bar{\tau}_{s,r}(x)}{(\rho_s-\rho)gD_{50}}, \tag{33}$$

where α_c is a non-dimensional coefficient.

The surface shear stress is estimated from Eq. (13), thus:

$$\bar{C}_a(x) = \alpha_c\rho_s\left[\frac{D_r(x)}{(\rho_s-\rho)gD_{50}C_\varphi(x)}\right]^3. \tag{34}$$

In this study, the numerical value $\alpha_c=1\times10^{-6}$ has been estimated from the Delta Flume'93 data (Test 1b) in order to get the best fit with the experimental data. Since the value of $\bar{C}_a(x)$ was measured at a single location every hour, only the value measured at the 17th hour is retained to find α_c. In fact, this value located on the outer bar (x=138 m) appears to be the highest over the profile.

8. Sensitivity analysis of the sediment transport and bed evolution models

To begin with, the influence of the turbulent diffusivity model and of the parametrization of the bottom concentration $\bar{C}_a(x)$ on the MSC distribution are analysed. Then, the influence on the suspended sediment flux of the $\bar{C}_a(x)$ parametrization and of the current and MWL model options is discussed. The cross-shore distribution of the total sediment flux $\bar{q}_t(x)$ is also analysed. Finally, the influence of the breaking roller and of the $\bar{C}_a(x)$ parametrization on the bed profile evolution is analysed. The data from Test 1b of the Delta-Flume'93 experiments are still used for comparison purposes.

8.1. Suspended sediment concentration

8.1.1. Influence of the turbulent diffusivity model

The vertical distribution of $\bar{C}(x, z)$ is computed using the three turbulent diffusivity models. For this set of tests, the measured near-bottom concentrations are used as the reference concentration $\bar{C}_a(x)$ in order to get rid of this additional parametrization. The computations are performed at the cross-shore locations where near-bottom concentration measurements are available (Fig. 11).

Using the uniform $\bar{\Gamma}_{t,1}$ and $\bar{\Gamma}_{t,2}$ parametrizations, the $\bar{C}(x, z)$ vertical profiles show the same behaviour, with an exponential decrease with height. For $\bar{\Gamma}_{t,1}$, a good agreement with experimental data is observed near the bed but the decrease in concentration with z is too large. The concentration from $\bar{\Gamma}_{t,2}$ is overestimated all over the depth at almost all the locations, except at P$_9$ where the agreement with experimental data is very good. In fact, the $\bar{\Gamma}_{t,2}$ model features a bottom shear stress induced turbulence which is too large, except for small water depths where this turbulence production should influence the entire water depth. The best agreement with the data is obtained with the $\bar{\Gamma}_{t,3}$ parametrization despite the fact that close to the surface, the model underestimates the concentration at

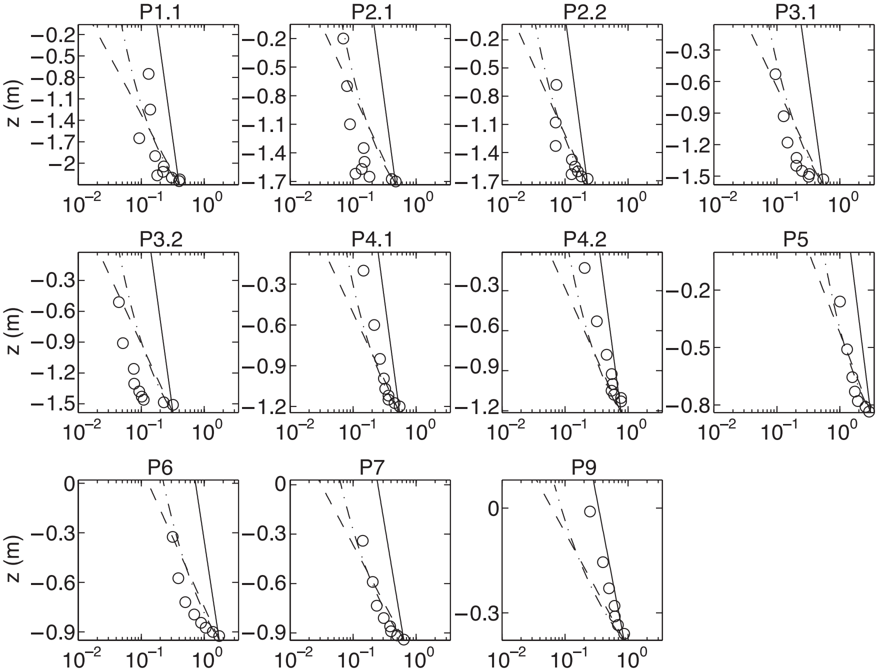

Fig. 11. Vertical profiles of the Mean Suspended Sediment Concentration (MSC) $\bar{C}(x, z)$ (kg/m^3). (– –) $\bar{\Gamma}_{t,1}(x)$: Eq. (5), (—) $\bar{\Gamma}_{t,2}(x)$: Eq. (6), (– · –) $\bar{\Gamma}_{t,3}(x, z)$: Eq. (9), (○) experimental data.

almost all locations. The results obtained with $\bar{\Gamma}_{t,3}$, in comparison with the one obtained from $\bar{\Gamma}_{t,1}$, show that the vertical variation of the wave bottom shear stress induced turbulence plays an important role on the $\bar{C}(x, z)$ vertical profiles especially from the mid-depth to the surface and should be taken into account.

One should notice that seaward of the outer bar the measured $\bar{C}(z)$ profiles exhibit a two layers vertical structure: $\bar{C}(z)$ strongly decreases in the bottom vicinity and then becomes almost constant up to the free surface. The numerical model cannot reproduce these two layers vertical profiles with the implemented turbulent diffusivity. Nevertheless, this effect could be introduced in the model by using a two layers turbulent diffusivity (Van Rijn, 1989), but this parametrization is not relevant in the surf zone.

8.1.2. Bed concentration

The cross-shore profiles of $\bar{C}_a(x)$ computed with the four parametrizations of the bed reference concentration $\bar{C}_a(x)$ at the 17th hour of Test 1b are plotted on Fig. 12. The experimental data are also plotted although we should bear in mind that only the highest value at x=138 m (t=17 h) is fully meaningful since it corresponds to the bottom profile used in the computations. Thus, only qualitative discussion can be done. An additional profile, $\bar{C}_{a,\mathrm{mes}}(x)$, has been derived from these experimental data interpolated along the entire cross-shore profile (splines). $\bar{C}_{a,\mathrm{mes}}(x)$ is used later for the suspended sediment flux estimation.

Despite their specific cross-shore variation, all the parametrizations for the reference concentration feature two maxima at the bars locations, except VR89 which only features the outer maximum and gives null values shoreward. The N86 and VR89 models (based on the Shields parameter computed from the wave motion) exhibit another maximum at $x \simeq 50$ m, the location where the $D_w(x)$ maximum has been observed (Fig. 4b). This behaviour has no physical meaning in terms of sediment transport because of the high water depth in this area ($d/L \gg 0.04$). The SM93 model seems to give a more realistic profile despite the very high values obtained for $\bar{C}_a(x)$. The SAT01 results exhibit the same kind of behaviour as SM93 seaward of the outer bar, but a better quantitative agreement is obtained. In fact, it is important to recall

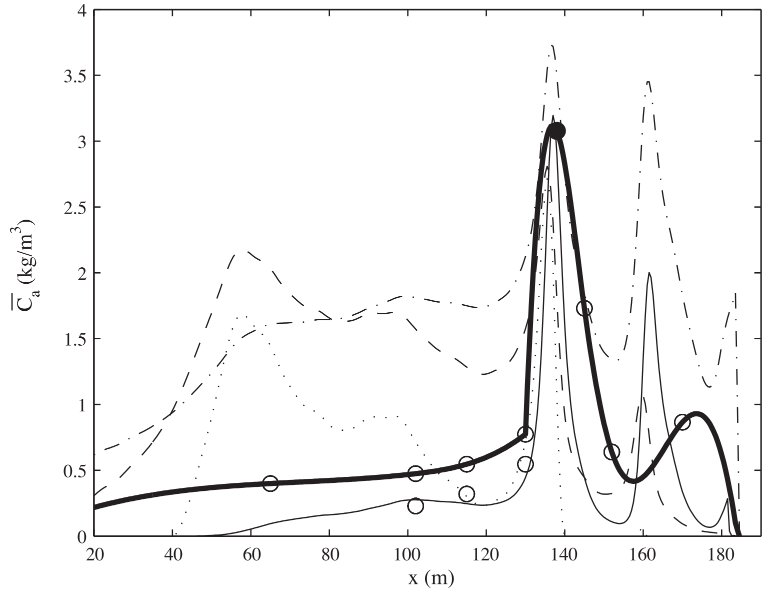

Fig. 12. Cross-shore distribution of the bed concentration, $\bar{C}_a(x)$, for the 17th hour of Test 1b with $x \in [20, 184]$; (—) Spielmann–Astruc–Thual (2001), (– –) Nielsen (1986), (· · ·) Van Rijn (1989), (– · –) Smith and Mocke (1993), (**—**) profile obtained by interpolating experimental data, $\bar{C}_{a,\mathrm{mes}}(x)$, (●) experimental data obtained at the 17th hour, (○) experimental data obtained at the other hours of Test 1b.

that the numerical value of $\alpha_c=10^{-6}$ (Eq. (34)) has been chosen to fit the maximum experimental value. Nevertheless, one can observe that SAT01 results seem to be in good agreement with experimental data obtained for $P_{2.2}$ (x=102 m), $P_{3.2}$ (x=115 m) and $P_{4.2}$ (x=130 m) shoreward to the outer bar.

A more detailed quantitative evaluation of the reference concentration models can be performed using experimental data. Figs. 13 and 14 show the experimental and the computed reference concentration $\bar{C}_a$ at each measurement locations. The SM93 parametrization yields to a significant overestimation of the bottom concentration at all locations. The VR89 formulation is in good agreement with the experimental data from P_1 to P_4. In the bars area, however, $\bar{C}_a$ is underestimated by this formula and even takes null value due to the threshold. The N86 parametrization strongly overestimates $\bar{C}_a$ seaward of the outer bar whereas, from P_5 to P_9, $\bar{C}_a$ is underestimated. The SAT01 model gives results which are close to the data except in the seaward region, at $P_{1.1}$, $P_{2.1}$ and $P_{3.1}$, where the concentration is too small. One can notice that between the bars, at P_6, all the models strongly underestimate the value of $\bar{C}_a$ except SM93.

From the results of these tests, the SAT01 model proved to improve significantly the estimation of the bottom sediment concentration in the nearshore area for this experimental case. However, a model calibration has to be done on several experimental data in order to better estimate α_c.

8.2. Suspended sediment transport rate

The aim of this section is to analyse the influence of both current and MWL model and reference concentration parametrization on the suspended sediment transport rate, $\bar{q}_s(x)$. With respect to the current, the influence of the selected resolution techniques (E1 and E2) as well as the impact of the breaking roller term should be evaluated. As there is no data for $\bar{q}_s(x)$, the bottom concentration experimental data, $\bar{C}_{a,\mathrm{mes}}(x)$, is used as a model input to estimate the suspended sediment flux which is thus only influenced by the current resolution technique. The resulting sediment flux is considered as the reference case.

In the tests, the turbulent diffusion models are $\bar{\nu}_{t,2}$ and $\bar{\Gamma}_{t,3}$ which take into account the wave and the roller turbulence production.

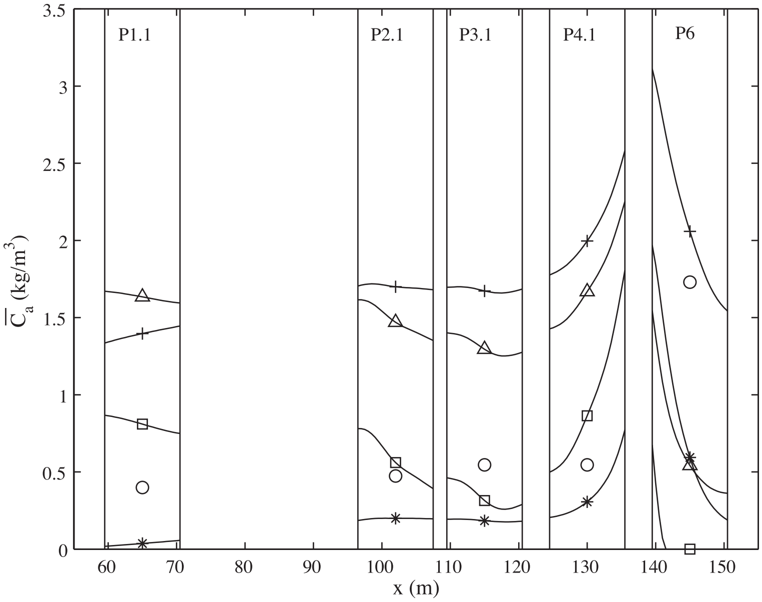

Fig. 13. Cross-shore variability of the simulated reference concentration, $\bar{C}_a(x)$, around (±5.5 m) the measurement locations, for $x \in [55, 155]$ and $t \in \{1,2,3,4,7\}$ (see Fig. 3). (△) Nielsen (1986) N86, (□) Van Rijn (1989) VR89, (+) Smith and Mocke (1993) SM93, (*) present study SAT01, (○) experimental data.

8.2.1. Influence of the current and MWL model

We have performed different simulations for the 17th hour of Test 1b using $\bar{C}_{a,\mathrm{mes}}(x)$: First, the E1R11 (i) and E2R11 (ii) resolution techniques are used for the current and MWL model and second, the influence of the roller contribution is tested using E2 technique: E2R11, E2R10 and E2R00.

The sediment fluxes estimated using E1 and E2 techniques are very similar with only a small difference (≤2%) for the maximum value of $|\bar{q}_\mathrm{s}|$ (Fig. 15). Both techniques thus proved to be equivalent in term of sediment transport rate even if they lead to different $\bar{u}(x, z)$ estimations. As underlined before, the E2 technique (zero bottom shear stress condition) is therefore a suitable technique to solve the mean momentum Eq. (10).

The three simulations performed to analyse the roller influence are now analysed in terms of $\bar{q}_\mathrm{s}(x)$ estimation (Fig. 15). A significant influence of the roller term should be noticed especially in the vicinity of the seaward bar (from $x \cong 130$ m to $x = 150$ m). The maximum of $|\bar{q}_\mathrm{s}|$ is 50 % higher when the roller is taken into account and is shifted shoreward like the maximum of $D_\mathrm{r}(x)$ and $\partial_x \eta(x)$. Moreover, when the roller term is only introduced to compute the setup (Eqs. (11.a) and (21)), a reduction in the maximum of $|\bar{q}_\mathrm{s}|$ is observed, together with a shoreward shift as expected. This decrease can be explained by a shift between the maxima of the two forcing term of Eq. (10). Taking into account the roller term in the depth-integrated mass balance (Eq. (11.b)) induces a strong increase of $|\bar{q}_\mathrm{s}|$ together with an additional shoreward shift of the $|\bar{q}_\mathrm{s}|$ maximum, an important feature for the bottom evolution. To conclude, whereas we already noticed that the horizontal current is overestimated outside the bars area when the roller terms are included, we show here that they should be taken into account in both Eqs. (11.b) and (21) in order to get a better estimate of the cross-shore variation of the suspended sediment transport rate for a barred beach profile.

8.2.2. Influence of the reference concentration model

E2 technique including the roller contribution is still used in the current and MWL model to perform the tests with the four $\bar{C}_a(x)$ models. We performed also a computation using $\bar{C}_{a,\mathrm{mes}}(x)$ in order to get an estimate for $\bar{q}_\mathrm{s}(x)$ for comparison purposes.

Fig. 16 shows the cross-shore distributions of the suspended sediment flux for the 17th hour of Test

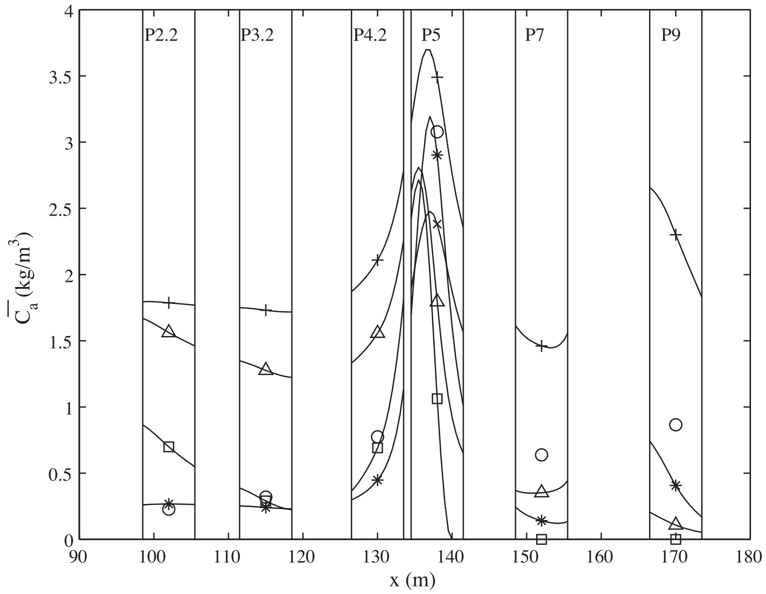

Fig. 14. Cross-shore variability of the simulated reference concentration, $\bar{C}_a(x)$, around (±3.5 m) the measurement locations, for $x \in [90, 180]$ and $t \in \{8, 10, 12, 15, 16, 17\}$ (see Fig. 3). (△) Nielsen (1986) N86, (□) Van Rijn (1989) VR89, (+) Smith and Mocke (1993) SM93, (*) present study SAT01, (○) experimental data.

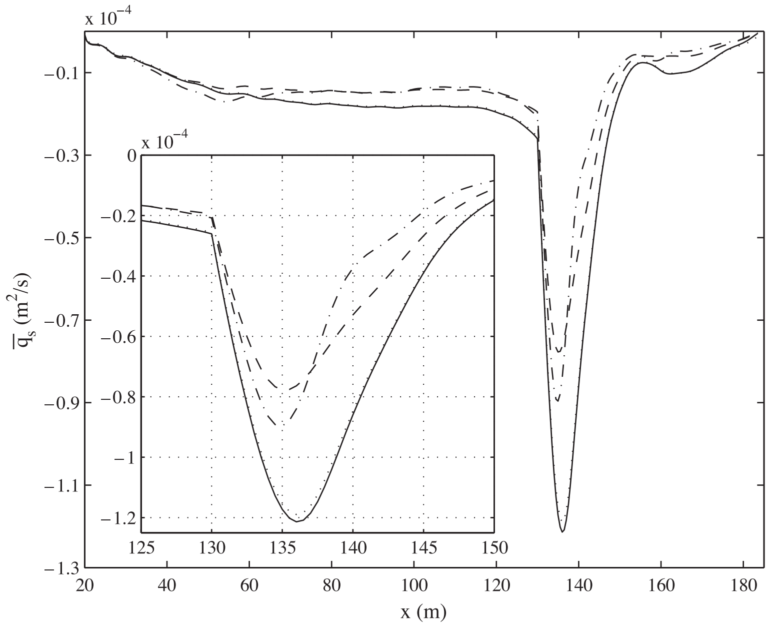

Fig. 15. Cross-shore profiles of the suspended sediment transport rate at t=17 h using the interpolated experimental bottom concentration ($\bar{C}_{a,\mathrm{mes}}(x)$). (—) E2R11 (Eqs. (21) and (11.b)), (– –) E2R10 (Eqs. (21) and (11.a)), (– · –) E2 (Eqs. (18) and (11.a)), (· · ·) E1R11 (Eqs. (21) and (11.b)).

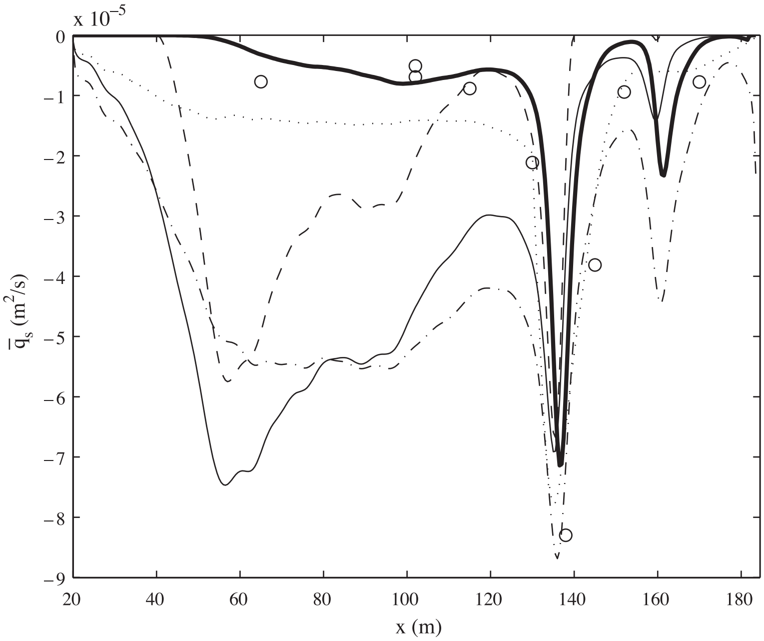

Fig. 16. Cross-shore suspended sediment transport rate profiles at t=17 h using E2R11. (—) Nielsen (1986) N86, (– –) Van Rijn (1989) VR89, (– · –) Smith and Mocke (1993) SM93, (**—**) present study SAT01, (· · ·) reference result ($\bar{C}_{a,\mathrm{mes}}(x)$ interpolated from experimental data).

1b. The very different $\bar{q}_\mathrm{s}(x)$ distributions exhibit cross-shore profiles similar to the bottom concentration $\bar{C}_a(x)$ for the related model (up to the sign) (Fig. 12). All $\bar{C}_a(x)$ models (except VR89) lead to a local maximum for $|\bar{q}_\mathrm{s}|$ over the inner bar, whereas the reference case does not, owing to the interpolation procedure. The VR89 model features a drastic increase of $\bar{q}_\mathrm{s}(x)$ seaward of the outer bar where $\bar{q}_\mathrm{s}(x)$ remains zero. This parametrization seems not to be appropriate to compute the bed evolution, at least in this case. However, it gives the best estimation of $\bar{q}_\mathrm{s}(x)$ decrease over the outer bar. The SAT01 model leads to a realistic $\bar{q}_\mathrm{s}(x)$ profile, especially seaward of the outer bar ($20 \le x \le 130$ m) even if $|\bar{q}_\mathrm{s}|$ is underestimated compared to the reference case. The SAT01 model also properly estimates the seaward maxima of $|\bar{q}_\mathrm{s}|$.

8.3. Total sediment transport rate

Before computing the bed evolution, the total sediment transport rate distribution $\bar{q}_\mathrm{t}(x)$ is analysed. Only $\bar{q}_\mathrm{t}(x)$ obtained from the interpolated experimental data $\bar{C}_a(x)$ and from the SAT01 model are discussed. The $\bar{q}_\mathrm{b}(x)$, $\bar{q}_\mathrm{s}(x)$ and $\bar{q}_\mathrm{t}(x)$ results are plotted in Fig. 17.

The bedload transport rate features a cross-shore distribution which is very similar to the $D_\mathrm{w}(x)$ distribution (see Fig. 4b). We can also notice that $\bar{q}_\mathrm{b}(x)$ and $|\bar{q}_\mathrm{s}(x)|$ are of the same order of magnitude. The total sediment transport rate from the SAT01 model is positive seaward of the outer bar as the sediment transport is mainly due to the wave motion. Over the bars, where the transport is mainly governed by the undertow, $\bar{q}_\mathrm{t}(x)$ is negative. In the trough, we observe a positive value for $\bar{q}_\mathrm{t}(x)$, which shows that the wave-driven transport is dominant. One can notice that $\partial_x \bar{q}_\mathrm{t}(x)$ is stronger for the SAT01 model than in the computation where $\bar{C}_{a,\mathrm{mes}}(x)$ is used, in particular shoreward of the outer bar.

8.4. Bed evolution

The morphodynamical computations are performed from t=1 h to t=17 h. The measured bottom profile at t=1 h is used as initial condition, and the wave and

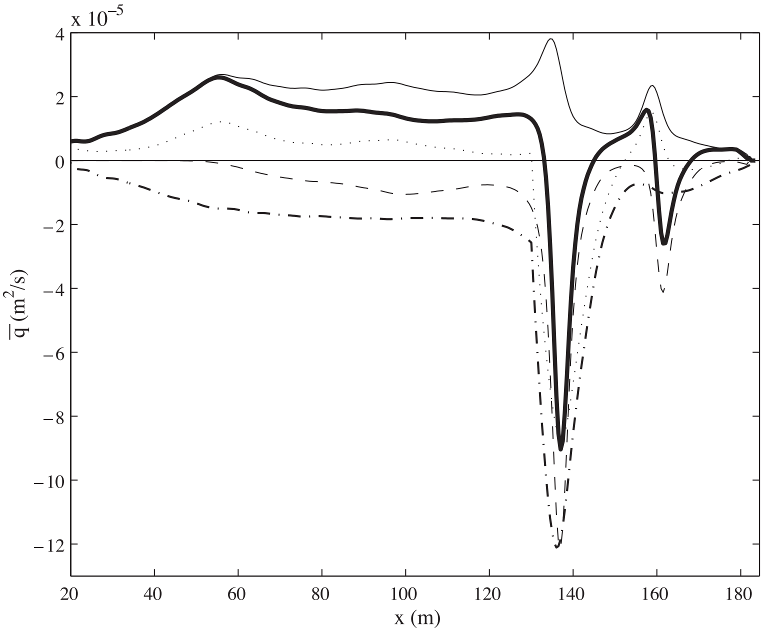

Fig. 17. Cross-shore profiles of the bedload, suspended and total sediment transport rates at t=17 h using E2R11. (—) $\bar{q}_{\rm b}(x)$, (– –) $\bar{q}_{\rm s}(x)$ with SAT01 model (present study) for $\bar{C}_a(x)$, (– · –) $\bar{q}_{\rm s}(x)$ with $\bar{C}_{a,\rm mes}(x)$, (**—**) $\bar{q}_{\rm t}(x)$ with SAT01 model for $\bar{C}_a(x)$, (· · ·) $\bar{q}_{\rm t}(x)$ with $\bar{C}_{a,\rm mes}(x)$.

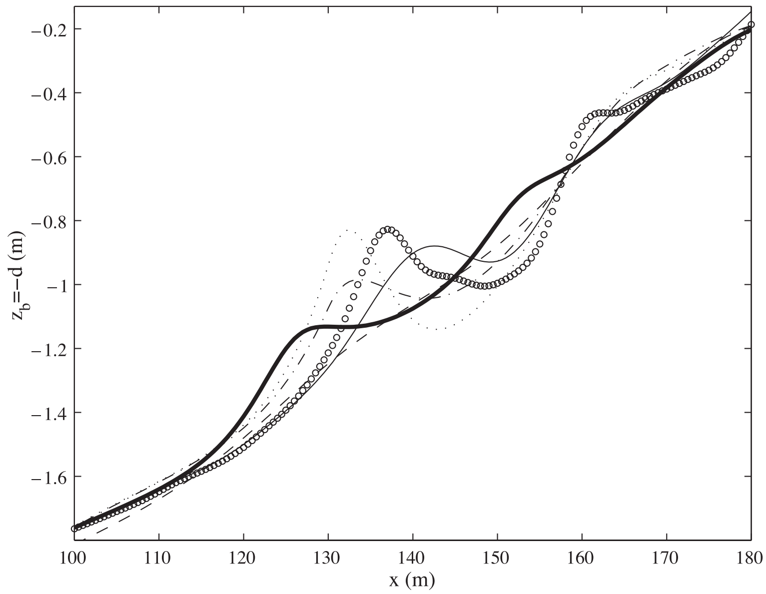

Fig. 18. Cross-shore bed profiles after 16 h of simulation using E2 technique for the current computation. (—) t=1 h measured, (○) t=17 h measured, (– –) t=17 h using $\bar{C}_a(x)$ given by N86 and E2R11, (—) t=17 h using $\bar{C}_a(x)$ given by SAT01 and E2R11, (· · ·) t=17 h using $\bar{C}_{a,\rm mes}(x)$ and E2R11, (– · –) t=17 h using $\bar{C}_{a,\rm mes}(x)$ and E2R00.

set-up characteristics at the seaward boundary are updated every hour using the experimental data. Fig. 18 shows the bottom profiles evolution.

The influence of the breaking roller on the bed evolution is tested using the E2 technique for the current and MWL model and $\bar{C}_{a,\mathrm{mes}}(x)$ reference concentration in order to get rid of the concentration parametrization. If the roller is taken into account, the bars and the trough exhibit a larger amplitude than without the roller term, in better agreement with the measurements. However, for both cases, a seaward shift of their location is observed in comparison to the experimental data.

According to these results, the roller contribution is taken into account when the N86 and SAT01 models are used. With the N86 model, the bars disappear. Although not shown here, the same phenomenon occurs for VR89 and SM93 parametrizations. The SAT01 model, however, keeps a bottom profile featuring two bars. Their shape is, however, smoother than in the experiments. As underlined in the analysis of the total sediment transport, the poor estimation of the current seaward of the outer bar may be responsible for this behaviour. Both bars experience a seaward motion, like in the experiments. However, this motion is faster than the motion observed in the experiments and in the computation using the $\bar{C}_{a,\mathrm{mes}}(x)$. The same behaviour has already been noticed in previous studies (Srinivas and Dean, 1996; Rakha et al., 1997).

9. Conclusion

We developed a deterministic beach profile model which has been used to compare several models for current and sediment concentration modelling. The intercomparison of the various parametrizations has been first performed for each individual physical process and then for the bed evolution. The data from the Delta Flume laboratory experiment, designed for validations and calibrations of this type of models, have been used as a reference.

The current and MWL model is based on the resolution of a 1D vertical diffusion equation for the mean horizontal velocity. We have carefully studied several approaches (E0, E1, E2, I1 and I2 techniques), which differ by the way boundary or integral conditions are specified. We have pointed out that the estimation of the mean water level from a vertically integrated momentum equation is equivalent to a condition on the difference between the surface and the bottom shear stresses. After a detailed study of the various techniques to solve the mean horizontal velocity and the mean water level (see Table 3), we show that E2 and I2 techniques give the best estimation when the roller contribution in the flow discharge condition is not taken into account (Eq. (11.a)) except in the trough area. In this region, the introduction of the roller term leads to a better agreement with experiments. Moreover, we show that I2 technique gives a better vertical structure of $\bar{u}(x, z)$, whereas using E2 technique, the intensity is better estimated. However, neither of these techniques properly solve the mean horizontal velocity in the boundary layer. Such a modelling would require a proper estimation of the term $\overline{\tilde{u}\tilde{w}}$. The turbulent viscosity influence is also analysed. We show that a uniform vertical profile is relevant to properly estimate the MHV vertical structure provided that the two main turbulence sources are taken into account.

In the sediment transport model, we have compared several turbulent diffusivity models for the 1D vertical diffusion equation governing the mean suspended concentration. We have shown that a linear turbulent diffusivity profile, taking into account the bottom wave shear stress as well as the surface wave breaking productions, gives the best results for this model. The weakness of the classical parametrizations for the reference concentration at the bottom have been pointed out. In fact, three classical parametrizations based on the Shields parameter constructed with the shear stress due to the wave bottom oscillatory velocity, one of them including the wave breaking influence through the roller dissipation rate, have been tested. A new parametrization based on a Shields parameter constructed from the surface shear stress due to the wave breaking, has been proposed. With this new bottom concentration formula, the bottom evolution model keeps the two bars morphology of the Delta Flume experiment, whereas the classical models yield to the disappearance of the bars. However, our model still leads to a too fast offshore motion of the bars, a bias already observed in other models (Srinivas and Dean, 1996; Rakha et al., 1997).

Acknowledgements

The authors wish to acknowledge the generous help of Dirk-Jan R. Walstra, engineer at Delft Hydraulics, The Netherlands, for providing the Delta Flume'93 data and the relevant report (Roelvink and Reniers, 1995). We acknowledge the financial support of the French PNEC ART7 program.

References

Arcilla, A.S., Roelvink, J.A., O'Connor, B.A., Reniers, A., Jiménez, J.A., 1994. The Delta Flume'93 experiments. Proc. Coastal Dynamics '94, Barcelona, Spain. ASCE, New York, pp. 488–502.

Bailard, J.A., Inman, D.L., 1981. An energetics bedload model for a plane sloping beach: local transport. J. Geophys. Res. 86 (C3), 2035–2043.

Battjes, J.A., 1983. Surf zone turbulence. Proc. 20th Int. Ass. Hydr. Res. Congr., Moscow, Seminar on Hydrodynamics of Waves in Coastal Areas.

Battjes, J.A., Janssen, J.P.F.M., 1978. Energy loss and set-up due to breaking of random waves. Proc. 16th Int. Conf. on Coastal Engineering, Hamburg. ASCE, New York, pp. 569–587.

Battjes, J.A., Stive, M.J.F., 1985. Calibration and verification of a dissipation model for random breaking waves. J. Geophys. Res. 90 (C5), 9159–9167.

Cox, D.T., Kobayashi, N., 1996. Undertow profiles in the bottom boundary layer under breaking waves. Proc. 25th Int. Conf. on Coastal Engineering, Orlando. ASCE, New York, pp. 3194–3206.

Deigaard, R., Fredsøe, J., 1989. Shear stress distribution in dissipative water waves. Coast. Eng. 13, 357–378.

Deigaard, R., Justesen, P., Fredsøe, J., 1991. Modelling of undertow by a one-equation turbulence model. Coast. Eng. 15, 431–458.

De Vriend, H.J., Kitou, N., 1990. Incorporation of wave effects in a 3D hydrostatic mean current model. Proc. 22nd Int. Conf. on Coastal Engineering, Delft. ASCE, New York, pp. 1005–1018.

De Vriend, H.J., Stive, M.J.F., 1987. Quasi-3D modelling of nearshore currents. Coast. Eng. 11, 565–601.

Grant, W.D., Madsen, O.S., 1979. Combined wave and current interaction with a rough bottom. J. Geophys. Res. 84 (C4), 1797–1808.

Haines, J.W., Sallenger, A.H., 1994. Vertical structure of mean cross-shore currents across a barred surf zone. J. Geophys. Res. 99 (C7), 14223–14242.

Hansen, J.Buhr, Svendsen, I.A., 1984. A theoretical and experimental study of undertow. Proc. 19th Int. Conf. on Coastal Engineering, Houston. ASCE, New York, pp. 2246–2262.

Hardy, T.A., Kraus, N.C., 1987. A numerical model for shoaling and refraction of second-order cnoidal waves over an irregular bottom. Technical report of US Army Engineering, W.E.S., CERC 87-9.

Jonsson, I.G., Carlsen, N.A., 1976. Experimental and theoretical investigations in an oscillatory rough turbulent boundary layer. J. Hydraul. Res. 14 (1), 45–60.

Kamphuis, J.W., 1975. Friction factor under oscillatory waves. J. Waterw., Port, Coast., Ocean Eng. Div. 101 (WW2), 135–144.

Longuet-Higgins, M., 1953. Mass transport in water waves. Philos. Trans. R. Soc. Lond. Ser. A: Math. Phys. Sci. 245 (903), 535–581.

Mocke, G.P., Reniers, A., Smith, G.G., 1994. A surfzone parameter sensitivity analysis on LIP11D suspended sediment and return flow measurements. Proc. on Coastal Dynamics'94, Barcelona. ASCE.

Nairn, R.B., Roelvink, J.A., Southgate, H.N., 1990. Transition zone width and implications for modelling surfzone hydrodynamics. Proc. 22nd Int. Conf. on Coastal Engineering, Delft. ASCE, New York, pp. 68–81.

Nielsen, P., 1986. Suspended sediment concentrations under waves. Coast. Eng. 10, 23–31.

Nielsen, P., 1992. Coastal bottom boundary layers and sediment transport. Advanced Series, vol. 4. World Scientific.

Rakha, K.A., 1998. A quasi-3D phase-resolving hydrodynamic and sediment transport model. Coast. Eng. 34, 277–311.

Rakha, K.A., Deigaard, R., Brøker, I., 1997. A phase-resolving cross shore sediment transport model for beach profile evolution. Coast. Eng. 31, 231–261.

Rivero, F.J., Arcilla, A.S., 1995. On the vertical distribution of $\langle\tilde{u}\tilde{w}\rangle$. Coast. Eng. 25, 137–152.

Rivero, F.J., Arcilla, A.S., 1997. Discussion-on the vertical distribution of $\langle\tilde{u}\tilde{w}\rangle$: reply to the comments of Z.J. You. Coast. Eng. 30, 311–315.

Roelvink, J.A., Brøker, I., 1993. Cross-shore profile models. Coast. Eng. 21, 163–191.

Roelvink, J.A. and Reniers, A.J.H.M., 1995. LIP 11D Delta Flume experiments: a dataset for profile model validation. Technical report H2130. WL/Delft Hydraulics, Delft, The Netherlands.

Roelvink, J.A., Stive, M.J.F., 1989. Bar-generating cross-shore flow mechanisms on a beach. J. Geophys. Res. 94 (C3), 4785–4800.

Smith, G.G., Mocke, G.P., 1993. Sediment suspension by turbulence in the surf zone. In: Bélorgey, M., Sleath, J.F.A. (Eds.), Sediment Transport Mechanisms in Coastal Environments and Rivers. World Scientific, pp. 375–387.

Srinivas, R., Dean, R.G., 1996. Cross-shore hydrodynamics and profile response modeling. Coast. Eng. 27, 195–221.

Stive, M.J.F., De Vriend, H.J., 1987. Quasi-3D nearshore current modelling: wave-induced secondary current. Proc. of a Special Conference on Coastal Hydrodynamics. ASCE, New York, pp. 356–370.

Stive, M.J.F., De Vriend, H.J., 1994. Shear stress and mean flow in shoaling and breaking waves. Proc. 24th Int. Conf. on Coastal Engineering, Kobe. ASCE, New York, pp. 594–608.

Stive, M.J.F., Wind, H.G., 1986. Cross-shore mean flow in the surf zone. Coast. Eng. 10, 325–340.

Svendsen, I.A., 1984a. Wave heights and set-up in a surf zone. Coast. Eng. 8, 303–329.

Svendsen, I.A., 1984b. Mass flux and undertow in a surf zone. Coast. Eng. 8, 347–365.

Svendsen, I.A., 1987. Analysis of surf zone turbulence. J. Geophys. Res. 92 (C5), 5115–5124.

Svendsen, I.A., Madsen, P.A., Hansen, J.Buhr, 1978. Wave characteristics in the surf zone. Proc. 16th Int. Conf. on Coastal Engineering. ASCE, New York, pp. 520–539.

Svendsen, I.A., Hemming, A., Hansen, J.Buhr, 1987. The interaction between the undertow and the boundary layer flow on a beach. J. Geophys. Res. 92 (C11), 11845–11856.

Swart, H., 1976. Predictive equations regarding coastal transports. Proc. 15th Int. Conf. on Coastal Engineering, Honolulu, Hawaii. ASCE, New York.

Ting, F.C.K., Kirby, J.T., 1994. Observation of undertow and turbulence in a laboratory surf zone. Coast. Eng. 24, 51–80.

Van Rijn, L.C., 1989. Handbook of sediment transport by currents and waves. Report H461, Delft Hydraulics, Delft, The Netherlands.

You, Z.J., 1996. The effect of wave-induced stress on current profiles. Coast. Eng. 23, 619–628.

You, Z.J., 1997. Discussion-on the vertical distribution of $\langle\tilde{u}\tilde{w}\rangle$ by F.J. Rivero and A.S. Arcilla: comments. Coast. Eng. 30, 305–310.